https://doi.org/10.5194/egusphere-2026-2680
Preprint. Discussion started: 28 July 2026

State–Forcing and Slope-Position Controls on Near-Surface Hillslope Wetting and Flood-Peak Variability in a Steep Mountain Catchment

Yi Ao[1,2], Yanjun Wang[1,2], Yangwen Jia[3], Bibo Huang[4], and Xiaorong Huang[1,2*]

[1]State Key Laboratory of Hydraulics and Mountain River Engineering, Sichuan University, Chengdu, Sichuan, 610065, China.
[2]College of Water Resource & Hydropower, Sichuan University, Chengdu, Sichuan, 610065, China.
[3]Department of Water Resources, China Institute of Water Resources and Hydropower Research (IWHR), Beijing, 100038, China.
[4]Chengdu Hydrological and Water Resources Survey Center, Chengdu, Sichuan, 610065, China.

Correspondence to: Xiaorong Huang(hxiaorong@scu.edu.cn)

Abstract. Rainfall–runoff response in steep, vegetated mountain catchments often varies strongly among events because rainfall input interacts with antecedent wetness, soil water redistribution, and transient hillslope–channel connectivity. Yet it remains unclear whether near-surface soil moisture profiles can indicate when hillslope wetting departs from a simple top-down sequence and whether such signals help explain flood-peak variability at the catchment outlet. We examined 30 rainfall–runoff events in the Ganwuli River basin using 15-minute rainfall records, outlet discharge, and soil moisture observations from three topographic positions with sensors at depths of 10–60 cm. Within this monitored near-surface profile, the 10–30 cm sensors were treated as upper monitored layers and the 40–60 cm sensors as lower monitored layers. Event responses were described using response occurrence, wetting magnitude, response lag, non-sequential wetting, and lower-layer early response. Across events, peak discharge increased primarily with total rainfall, whereas the maximum hydrograph rise rate was more sensitive to the intensity of short-duration rainfall. Soil moisture responses were frequent in the upper monitored layers at the foot-slope position. By contrast, lower monitored layers at the mid-slope and upper-slope positions more often showed early or near-synchronous responses relative to the upper layers, indicating that wetting within the monitored profile was not always governed by sequential vertical propagation. Segmented logistic models and two-dimensional probability surfaces further indicated that these lower-layer responses were most likely to occur when wet antecedent conditions coincided with high short-duration rainfall intensity. Events with lower-layer early responses at the upper-slope position tended to have larger flood peaks, but this relationship is interpreted as an indicator of changing hillslope connectivity rather than direct evidence of deep groundwater flow paths. These findings suggest that high-frequency near-surface soil moisture profiles can add useful process information for interpreting event-scale flood variability, while deeper storage and groundwater mechanisms require independent observations.

https://doi.org/10.5194/egusphere-2026-2680
Preprint. Discussion started: 28 July 2026

1 Introduction

Small mountainous watersheds are prone to flash floods characterized by rapid hydrograph responses to intense, short-duration rainfall. Thresholds governing infiltration, subsurface runoff generation, and hillslope-channel connectivity are key factors controlling flood peak magnitude and timing. Recent studies indicate that even under similar rainfall inputs, non-linear rainfall-runoff responses are significantly amplified by the rapid expansion of the contributing area and the sudden activation of subsurface flow paths (Han et al., 2020; Zhang et al., 2023). Therefore, identifying the spatial and temporal activation of these subsurface pathways across different slope positions is essential for explaining mountainous flood mechanisms and improving event-based runoff parameterization.

Soil moisture observations are often used to place rainfall events in their antecedent hydrological context. Their value is not simply that wetter soils produce larger runoff responses, but that the effect of rainfall depends on how close the hillslope is to a hydrological threshold before the event begins. Cain et al. (2022) showed this clearly in threshold-controlled runoff generation, where antecedent wetness and event precipitation acted together rather than as separate predictors. Similar behaviour has been reported in hillslope experiments, where rainfall type and antecedent soil moisture jointly controlled the onset and strength of runoff response(Wang et al., 2022). These findings provide the basis for treating soil moisture not as a passive state variable, but as a condition that governs whether rainfall is stored locally, redistributed within the soil profile, or transferred more efficiently downslope.

This interpretation must be separated from processes occurring below the monitored soil profile. Salve et al. (2012) showed that rainfall can rapidly affect rock moisture and perched groundwater in weathered, fractured bedrock beneath a steep hillslope, demonstrating that storm response may involve storage and flow paths well below the shallow soil. More recent work has further shown that subsurface flow dynamics can be shaped by bedrock structure and vegetation cover at the hillslope scale(Uhlemann et al., 2024). These studies define the broader critical-zone context for interpreting rapid storm response, but they also mark an important observational limit for the present study. Sensors installed only within the upper 60 cm cannot resolve rock moisture, perched groundwater, or deeper bedrock flow. They can, however, show whether wetting within the monitored near-surface profile follows a sequential top-down pattern or whether lower monitored layers respond earlier than expected. Such timing departures are therefore treated here as near-surface indicators of changing hillslope connectivity, not as direct evidence of deep groundwater flow.

Recent high-frequency soil moisture studies have shown that wetting responses can vary strongly with slope position, soil depth, rainfall type, and antecedent state. In steep subtropical hillslopes, Lu et al. (2024) found that soil moisture responses differed among topographic positions, reflecting contrasts in local storage, drainage, and lateral redistribution. Zhang et al. (2024) further showed that rapid infiltration on complex hillslopes can be identified from the timing and magnitude of soil moisture response at multiple depths. The review by Nimmo et al. (2025) also emphasized that soil moisture time series can be used to detect preferential flow, but only when the limits of sensor depth, sampling interval, and spatial representativeness

https://doi.org/10.5194/egusphere-2026-2680
Preprint. Discussion started: 28 July 2026

are made explicit. Together, these studies suggest that high-frequency soil moisture profiles are most useful when they are used not as direct measurements of deep flow paths, but as indicators of how near-surface wetting is organized during events. A remaining gap is the link between these profile-scale wetting patterns and flood response at the catchment outlet. Many studies have examined either soil moisture controls on hillslope response or rainfall controls on streamflow generation, but fewer have tested whether non-sequential wetting within a monitored near-surface profile is associated with flood-peak magnitude and hydrograph rise rate. This question is particularly relevant in steep, humid catchments, where the effective contributing area may expand rapidly once antecedent wetness is high and rainfall intensity exceeds local infiltration or redistribution capacity. In such settings, lower-layer early response within the monitored profile may not prove deep groundwater flow, but it may still provide a useful event-scale signal of changing hillslope connectivity.

The Ganwuli River basin, located along the western margin of the Sichuan Basin, is a steep, densely vegetated mountain catchment affected by frequent summer floods. This study uses 15 min rainfall records, outlet discharge, and soil moisture observations from three topographic positions, namely the foot-slope, mid-slope, and upper-slope positions, during the 2023–2025 flood seasons. Sensors were installed at 10–60 cm depth. Within this near-surface monitored profile, the 10–30 cm sensors are defined as upper monitored layers and the 40–60 cm sensors as lower monitored layers. The study examines how topographic position and relative depth control the occurrence, magnitude, and timing of soil moisture response. It then tests whether non-sequential wetting and lower-layer early response are linked to antecedent wetness and short-duration rainfall intensity, and whether these signals are associated with peak discharge and hydrograph rise rate at the catchment outlet. The purpose is not to infer deep groundwater dynamics from shallow sensors, but to assess whether high-frequency near-surface soil moisture profiles can add process information for interpreting event-scale flood variability in steep mountain catchments.

2 Research Area and Data

2.1 Research Area Overview

The Ganwuli River basin is located on the western margin of the Sichuan Basin (103°25′–103°36′E, 30°45′–30°52′N). The basin has a drainage area of about 108 km², a main-channel length of approximately 22 km, and an average channel gradient of 5.8‰. The Heping Hydrological Station controls an upstream area of 78.7 km² and provides the outlet discharge record used in this study. The catchment has a humid subtropical monsoon climate. Mean annual air temperature is about 15 °C, with monthly means of approximately 24 °C in July and 4 °C in January. Annual precipitation is generally 1200–1900 mm, with most rainfall occurring during the summer flood season. Vegetation cover exceeds 90%, and the steep terrain produces marked local differences in rainfall, soil wetness, and drainage conditions. The catchment, station network, and soil moisture monitoring layout are shown in Fig. 1.

https://doi.org/10.5194/egusphere-2026-2680
Preprint. Discussion started: 28 July 2026

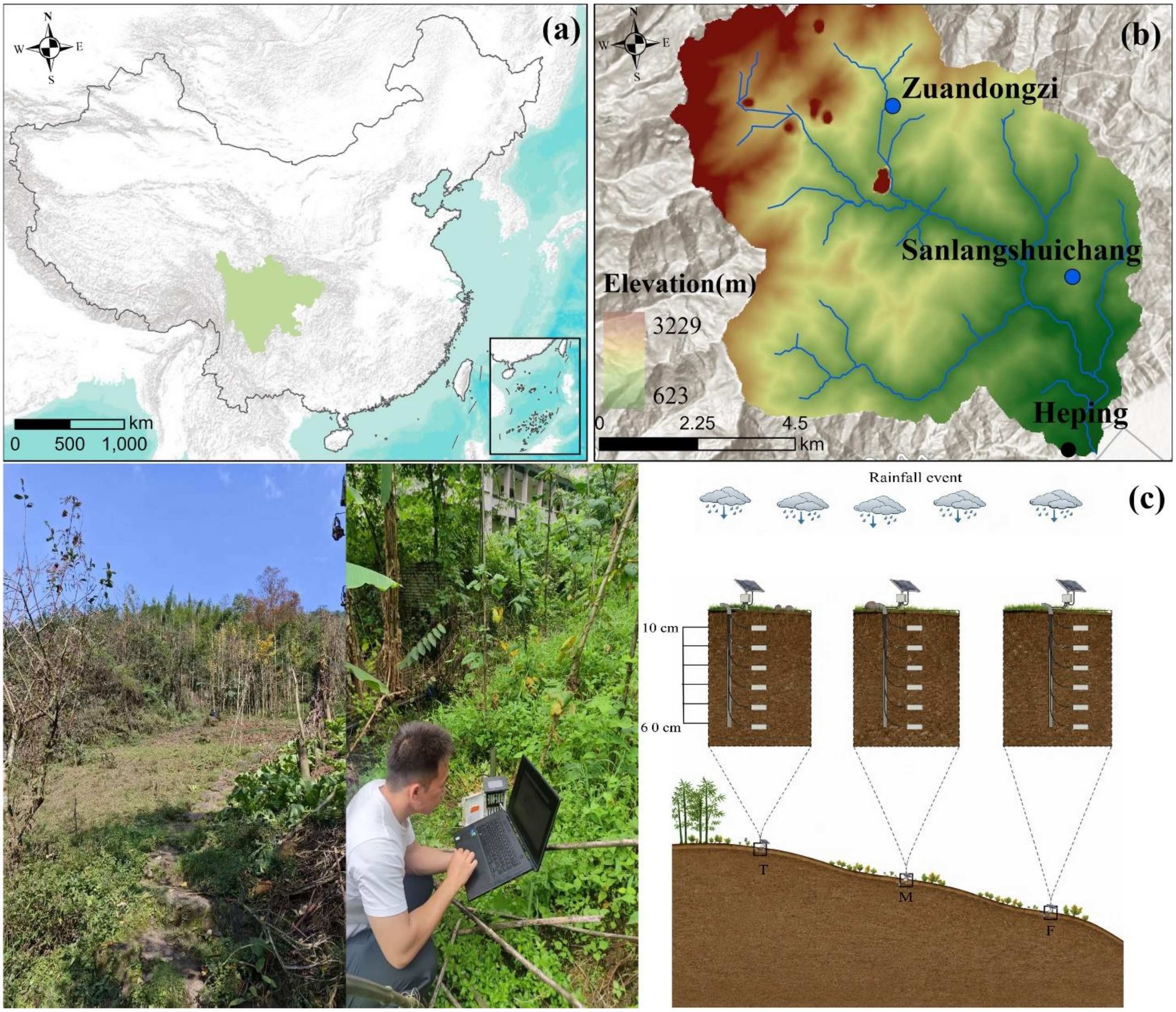

Fig. 1. Study catchment, hydrometeorological stations, and soil moisture monitoring layout. (a) Location of Sichuan Province and the Ganwuli River basin. (b) Catchment boundary and station network, including rainfall stations and the Heping Hydrological Station. (c) Local monitoring layout at the hillslope site, showing the three topographic positions and sensor depths within the upper 60 cm soil profile.

2.2 Observation Network

The observation network combined station rainfall, outlet discharge, and hillslope soil moisture measurements. Rainfall was recorded at Heping, Zuandongzi, and Sanlangshuichang stations at a 5 min interval during 2023–2025. The 5 min rainfall data were aggregated to 15 min totals to match the soil moisture sampling interval. Event rainfall descriptors, including total rainfall, duration, mean intensity, and peak short-duration intensity, were calculated from the 15 min rainfall series.

https://doi.org/10.5194/egusphere-2026-2680
Preprint. Discussion started: 28 July 2026

Streamflow data were obtained from the Heping Hydrological Station. Hourly water level and discharge records were available for the flood seasons from 1 May to 31 October in 2023–2025. These records were used to identify flood responses at the catchment outlet and to calculate peak discharge and hydrograph rise metrics. Because the discharge data are hourly, outlet response metrics were interpreted at the event scale rather than at the same temporal resolution as the soil moisture measurements.

Soil moisture was monitored at a hillslope site near Zuandongzi from 2 April 2024 onward. Three topographic positions were instrumented along a local hillslope monitoring line: foot-slope, mid-slope, and upper-slope. At each position, volumetric water content was measured every 15 min at six depths, namely 10, 20, 30, 40, 50, and 60 cm. In this study, the 10–30 cm sensors are referred to as the upper monitored layers, and the 40–60 cm sensors as the lower monitored layers. The monitoring design allows event-scale comparison of wetting occurrence, magnitude, and timing among topographic positions and relative depth classes within the upper 60 cm soil profile.

Table 1 Location and elevation of the three soil moisture monitoring positions.

Sites	Longitude	Latitude	Altitude (m)	Horizontal distance from slope foot (m)	Relative elevation (m)	Note
Slope foot(F)	103.452401	30.836173	1014.393	0	0	Starting point of slope monitoring profile
Mid-slope(M)	103.452506	30.836375	1025.903	24.5	11.5	About 25 m from the slope foot, with an elevation gain of about 11.5 m
Slope top(T)	103.452664	30.836635	1052.864	57.2	38.5	About 57 m from the slope foot, with an elevation gain of about 38.5 m

2.3 Data Preprocessing

All rainfall, discharge, and soil moisture records were checked and placed on a consistent time basis before event analysis. Rainfall totals were aggregated from 5 min to 15 min intervals. Soil moisture data were screened for physically unrealistic values and abrupt isolated spikes. Short gaps of no more than 2 h were filled by time interpolation when the neighbouring values were continuous and physically plausible. Longer gaps were retained as missing values and were not interpolated across discontinuities. Events with missing soil moisture data at any of the three positions or six depths within the analysis window were excluded from comparisons that required complete multi-depth profiles.

Rainfall events were defined from the 15 min rainfall record at the Zuandongzi station, which is closest to the hillslope monitoring site. Adjacent rainfall periods were merged when the intervening rain-free interval was shorter than 6 h. Candidate events were required to have total rainfall of at least 10 mm. For each event, the analysis window extended from 2 h before

https://doi.org/10.5194/egusphere-2026-2680
Preprint. Discussion started: 28 July 2026

rainfall onset to 6 h after rainfall cessation. The pre-event period was used to estimate antecedent soil moisture, whereas the post-event extension allowed delayed wetting responses to be included. A candidate event was retained only when the full soil moisture profile was available at all three topographic positions and when at least one sensor showed a detectable response. This screening reduced the influence of weak rainfall events and sensor noise on the response statistics.

Antecedent moisture was defined as the mean volumetric water content during the 2 h period before rainfall onset. A detectable soil moisture response was identified when the volumetric water content exceeded the antecedent value by at least 0.01 m^3 m^{-3} within the event window. For each responding sensor, the response magnitude was calculated as the maximum change in volumetric water content within the window, and the response lag was calculated as the time between rainfall onset and the first exceedance of the response threshold. The time difference between peak rainfall intensity and peak soil moisture was also calculated to describe the phase relation between rainfall forcing and local wetting. These definitions were used only to identify event-scale wetting responses within the monitored 0–60 cm profile.

3 Methods

3.1 Rainfall event identification and effective sample selection

All rainfall and soil moisture series were analysed at a common time step of $\Delta t = 15$ min. The original 5 min rainfall amounts were accumulated over complete 15 min windows to obtain the rainfall sequence $P(t)$ (mm 15 min^{-1}). The volumetric water content at slope position j and soil layer depth k is denoted as $\theta_{j,k}(t)$ (m^3 m^{-3}), where $j \in (F, M, T)$ represents the slope foot, mid-slope, and slope top, respectively, and $k \in (10,20,30,40,50,60)$ cm.

The soil moisture series were screened for values outside the physically plausible range of 0-0.60 (m^3 m^{-3}). Isolated abrupt changes that could be attributed to sensor malfunction were flagged and treated as missing values. This screening was intended to reduce the influence of instrument noise on response timing and magnitude, rather than to smooth short-term hydrological responses.

Rainfall events were defined from $P(t)$ using a baseline inter-event dry period of IETD_0= 6 h. Rainfall periods separated by a rain-free interval shorter than IETD_0 were merged into the same event. For event e, the start time $t_0(e)$ was defined as the beginning of the first 15-minute window with $P(t) > 0$, and the event end time $t_{\text{end}}(e)$ was defined as the end of the last such window. Event rainfall was described using total rainfall, duration, mean rainfall intensity, peak 15 min rainfall intensity, and rainfall concentration.

Total rainfall is defined as

$$P_{tot}(e) = \sum_{t \in e} P(t) \,, \tag{1}$$

The duration is defined as

$$D(e) = t_{end}(e) - t_0(e) \,, \tag{2}$$

https://doi.org/10.5194/egusphere-2026-2680
Preprint. Discussion started: 28 July 2026

The average rainfall intensity is defined as

$$AI(e) = \frac{P_{tot}(e)}{D(e)}, \quad (3)$$

Peak rainfall intensity is defined as

$$PI_{15}(e) = \max_{t \in e} P(t), \quad (4)$$

The corresponding hourly equivalent is $PI_h(e) = 4\,PI_{15}(e)$(mm h^{-1}). Rainfall concentration describes the degree to which rainfall is concentrated within a short part of the event and is defined as

$$CI(e) = \frac{P_{30}(e)}{P_{tot}(e)}, \quad (5)$$

$P_{30}(e)$ represents the maximum cumulative rainfall over a 30-minute period within the event.

To include both the initial wetting response and delayed redistribution within the monitored soil profile, the event analysis window was defined as

$$W(e) = [t_0(e) - 2h, t_{end}(e) + 6h], \quad (6)$$

The 2-hour window preceding the event stabilizes estimates of prior moisture content, while the 6-hour window following captures peak lag and redistribution. Valid events are screened based on water volume constraints, data integrity, and response discernibility: First, events with $P_{\mathrm{tot}}(e) \geq 10$ mm were retained as candidates. Subsequently, all six depth measurements $\theta_{j,k}(t)$ at three slope positions within $W(e)$ were required to be continuously available. Additionally, at least one slope position and depth must satisfy the discernible response criterion. This screening ensures consistency in indicator calculations across different slope positions and depths.

3.2 Event-scale response metrics for the monitored soil profile

Soil moisture responses were described using antecedent moisture, response occurrence, response lag, wetting magnitude, peak-to-peak phase difference, and apparent wetting-front velocity. All metrics were calculated within the monitored 0–60 cm near-surface soil profile. In this study, the sensors at 10–30 cm are referred to as the upper monitored layers, and those at 40–60 cm are referred to as the lower monitored layers.

First, AMC is defined as the average moisture content over the preceding 2 hours:

$$AMC_{j,k}(e) = mean\theta_{j,k}(t), t \in \left[t_0(e) - 2h, t_0(e)\right), \quad (7)$$

To ensure robust response discrimination and avoid interference from minor sensor noise, the minimum resolvable response threshold is defined as $\delta_\theta = 0.01$ (m^3 m^{-3}). When there exists $t \in W(e)$ such that

$$\theta_{j,k}(t) \geq AMC_{j,k}(e) + \delta_\theta, \quad (8)$$

https://doi.org/10.5194/egusphere-2026-2680
Preprint. Discussion started: 28 July 2026

Then it is determined that slope position j and depth k responded during event e, and the response indicator $R_{j,k}(e) = 1$ is recorded; otherwise, $R_{j,k}(e) = 0$.

T_i characterizes the onset time of infiltration triggering and the arrival of the wetting front at this depth, defined as the time difference until the threshold is first reached:

$$T_{i,j,k}(e) = min\{t - t_0(e) \mid \theta_{j,k}(t) \geq AMC_{j,k}(e) + \delta_\theta, t \in W(e)\}, \tag{9}$$

When $R_{j,k}(e) = 0$, $T_{i,j,k}(e)$ is recorded as missing and excluded from continuous indicator statistics but included in incidence statistics.

$\Delta\theta$ characterizes the net moisture increment and process intensity of an event. The peak increment is defined as

$$\Delta\theta^+_{j,k}(e) = max_{t\in W(e)}\theta_{j,k}(t) - AMC_{j,k}(e), \tag{10}$$

To reflect the impact of pullbacks and redistributions within events on volatility, while simultaneously calculating the range of extremes.

$$\Delta\theta_{j,k}(e) = max_{t\in W(e)}\theta_{j,k}(t) - min_{t\in W(e)}\theta_{j,k}(t), \tag{11}$$

Additionally, to enhance sensitivity to persistent rainfall and long-term redistribution, this study calculates the cumulative increment of events.

$$A_{\theta,j,k}(e) = \sum_{t\in W(e)} max\left[\theta_{j,k}(t) - AMC_{j,k}(e), 0\right] \cdot \Delta t, \tag{12}$$

Where Δt is measured in hours, the unit of A_θ is (m^3 m^{-3} h).

T_{p2p} characterizes the temporal offset between rainfall structure and peak water content response. Let $t_{PI}(e)$ denote the time at which the peak rainfall intensity occurs within the event.

Let $t_{\theta,\max}(j,k,e)$ denote the time at which $\theta_{j,k}(t)$ attains its maximum value within $W(e)$, then

$$T_{p2p,j,k}(e) = t_{\theta,max}(j,k,e) - t_{PI}(e), \tag{13}$$

When $T_{p2p} > 0$, it indicates that the peak moisture lags behind the peak precipitation; when $T_{p2p} \approx 0$, it indicates that the two are nearly synchronous; when $T_{p2p} < 0$, the local soil moisture peak occurs before the rainfall-intensity peak. In this study, negative or near-synchronous phase differences are interpreted as timing evidence of non-sequential wetting or local redistribution within the monitored 0–60 cm profile.

For adjacent sensor depths, an apparent wetting-front velocity was calculated only when both layers responded and when the response in the lower layer lagged behind the response in the upper layer. With $\Delta z = 10$cm between adjacent sensors, then

$$V_{wf,j,k\rightarrow k+1}(e) = \Delta z / \left[T_{i,j,k+1}(e) - T_{i,j,k}(e)\right], \tag{14}$$

https://doi.org/10.5194/egusphere-2026-2680
Preprint. Discussion started: 28 July 2026

When $T_{i,j,k+1} - T_{i,j,k} > 0$, V_{wf} is positive, indicating apparent downward propagation from an upper monitored layer to the adjacent lower monitored layer. When this difference is less than or equal to the sampling tolerance, the pair is treated as a non-sequential timing case.

3.3 Sequential and non-sequential wetting types

Under a simple sequential vertical wetting pattern, T_i is expected to increase with depth. Because soil moisture was sampled every 15 min, one sampling interval was used as the timing tolerance. At topographic position j, an event was classified as sequential when all adjacent responding layers satisfied

$$T_{i,j,k+1}(e) - T_{i,j,k}(e) > \Delta t \ , \quad (15)$$

This case indicates that wetting within the monitored profile was consistent with downward propagation from upper to lower monitored layers. If at least one adjacent pair satisfied

$$T_{i,j,k+1}(e) - T_{i,j,k}(e) \leq \Delta t \ , \quad (16)$$

the event was classified as non-sequential at position j. This category indicates that at least one lower monitored layer responded nearly synchronously with, or earlier than, the layer above it.

To identify stronger departures from the upper-to-lower wetting sequence, the lower monitored layer set was defined as $Z_l = (40,50,60)$cm and the upper monitored layer set as $Z_u = (10,20,30)$cm. If there exist $z_l \in Z_l$ and $z_u \in Z_u$ such that

$$T_{i,j,z_l}(e) \leq T_{i,j,z_u}(e) - \Delta t \ , \quad (17)$$

the event was marked as a lower-layer early response at position j. This event label is denoted as $DF_j(e) = 1$ to maintain consistency with subsequent analyses. Otherwise, $DF_j(e) = 0$. Here, DF refers only to lower-layer early response within the monitored 0–60 cm profile and does not imply direct observation of deep hillslope storage or groundwater flow.

At the event-sample level, the response occurrence rate for each topographic position and depth was calculated as

$$p_{R,j,k} = (1/N) \sum\nolimits_e R_{j,k}\,(e) \ , \quad (18)$$

For each topographic position, the lower-layer early response rate was calculated as

$$p_{DF,j} = (1/N) \sum\nolimits_e D\,F_j(e) \ , \quad (19)$$

To quantify the degree of departure from sequential wetting, the number of adjacent layer pairs that violated monotonic increase in T_i was recorded as n_{inv}. The sequential consistency index was then defined as

$$SI = 1 - n_{inv}/5 \ , \quad (20)$$

The denominator 5 is the number of adjacent depth pairs in the six-layer monitored profile. An SI value closer to 1 indicates a process closer to sequential infiltration, while a smaller SI value indicates a stronger non-sequential characteristic.

https://doi.org/10.5194/egusphere-2026-2680
Preprint. Discussion started: 28 July 2026

3.4 Control factor and threshold identification

Several observations within the same rainfall event share the same event forcing and are therefore not statistically independent. To account for this intra-event dependence, event identity was treated as a random effect. Mixed-effects models were used to estimate how topographic position, sensor depth, antecedent moisture, and rainfall forcing were related to response occurrence, wetting magnitude, and response timing.

For continuous response indicators ($\Delta\theta^+$, T_i, T_{p2p}, V_{wf} or SI), the general linear mixed-effects model was:

$$y_{j,k}(e) = \beta_0 + \beta_1 Pos_j + \beta_2 z_k + \beta_3 (Pos_j \times z_k) + \beta_4 AMC_{j,k}(e) + \beta_5 PI(e) + u_e + \varepsilon_{j,k}(e) \ , \tag{21}$$

Here, Pos_j is the categorical topographic-position term, z_k represents depth (cm), $u_e \sim N(0, \sigma_u^2)$ is the event random intercept, and ε is the residual term. For continuously distributed responses with significant skewness and strictly positive values ($\Delta\theta^+$, T_i), natural logarithmic transformations were applied to mitigate heteroscedasticity. For T_{p2p} (which can be either positive or negative) and SI (with restricted range), direct modeling using original units was employed. Fixed-effect coefficients and 95% confidence intervals are reported.

For the binary response variables, namely response occurrence $R_{j,k}(e)$ and lower-layer early response $DF_j(e)$, generalized linear mixed-effects models with a logit link were used:

$$logit[Pr(R_{j,k}(e) = 1)] = \alpha_0 + \alpha_1 Pos_j + \alpha_2 z_k + \alpha_3 AMC_{j,k}(e) + \alpha_4 PI(e) + u_e \ , \tag{22}$$

$$logit[Pr(DF_j(e) = 1)] = \gamma_0 + \gamma_1 Pos_j + \gamma_2 A\bar{M}C_j(e) + \gamma_3 PI(e) + u_e \ , \tag{23}$$

$A\bar{M}C_j(e)$ denotes the profile-averaged prior moisture content at slope position j.

For threshold identification, using R and DF as target events, univariate piecewise terms are constructed for AMC or PI_{15} within the GLMM framework. By performing grid searches over candidate threshold sets, the change point τ is identified via AIC minimization, thereby characterizing the structural change in the response probability-forced relationship when the state variable crosses τ. To preserve the correlated structure of multi-depth-multi-slope observations within events, event-scale bootstrap resampling is employed to estimate the 95% confidence interval for τ. Each resampling draws an event set while retaining all slope-depth observations. A two-dimensional smoothing model is further employed to fit $\Pr(DF = 1) = f(AMC, PI)$. Specifically, a binary response model is constructed using logit-linked two-dimensional thin-plate spline/tensor product spline smoothing terms. Cross-validation grouped by events evaluates generalization performance to mitigate overfitting risks. Discriminative capability is characterized by AUC, while probability calibration is assessed via Brier score and calibration curves. Gradient-boosted decision trees (GBDT) were used as a supporting sensitivity analysis to check whether the relative importance of AMC, PI, P_{tot}, D, CI, topographic position, and depth was consistent with the mixed-effects models and probability-surface results.

https://doi.org/10.5194/egusphere-2026-2680
Preprint. Discussion started: 28 July 2026

3.5 Linking monitored-profile responses with outlet flood characteristics

To examine whether near-surface wetting responses were associated with catchment-scale flood behaviour, flood characteristics were extracted from events with discharge observations at the Heping Hydrological Station. These included peak discharge Q_{peak}, time to peak T_{rise}, event runoff depth Q_e, and runoff coefficient $C = Q_e/P_{\text{tot}}$. This study approximated baseflow using the median flow rate from the 24 hours preceding the event:

$$Q_b(e) = median Q(t), t \in \left[t_0(e) - 24h, t_0(e)\right), \tag{24}$$

Event runoff depth calculation is

$$Q_e(e) = (1/A) \sum_{t\in[t_0,t_q]} max(Q(t) - Q_b(e), \; 0) \cdot \Delta t \times 1000, \tag{25}$$

Where A is the control area (m^2), Δt is the runoff time step (s), multiplied by 1000 to convert units from m to mm, and t_q is the end time of the event runoff process (which can be a fixed duration after rainfall cessation or the moment when flow recedes to near baseflow). Subsequently, aggregate slope indicators at the event scale (e.g., $\Delta\theta^+$, p_{DF}, V_{wf} or SI) are calculated. With P_{tot} and PI_{15} used as reference rainfall controls, the analysis tested whether monitored-profile response metrics were associated with Q_{peak} and the flood rise process. These associations were not interpreted as direct causal flow paths from the monitored soil layers to the catchment outlet.

3.6 Model diagnostics and uncertainty analysis

(1) Estimation and diagnostic principles

Linear mixed-effects models were estimated using maximum likelihood or restricted maximum likelihood methods. Residual normality and homoscedasticity are assessed via residual-predicted value scatter plots and Q-Q residual plots. When significant heteroscedasticity is present, log transformation of response variables ($\Delta\theta^+, T_i$) is prioritized before fitting, with direction consistency between transformed and untransformed data simultaneously reported. Regarding random effects structure, this study adopts u_e as the baseline structure and tests whether adding random slopes significantly improves model fit when necessary. Model comparison employs likelihood ratio tests and information criteria (AIC/BIC).

(2) Collinearity control and variable selection

To mitigate the impact of collinearity among rainfall characteristic variables on interpretability, variance inflation factors (VIF) are calculated prior to model entry. When VIF is significantly elevated, prioritize retaining variable combinations with clearer physical meaning and greater importance in the explanatory chain (typically centered on AMC and PI_{15}, supplemented by P_{tot} or CI). The conclusions are validated through alternative variable sensitivity comparisons to ensure independence from specific rainfall type indicator definitions.

(3) Binary model performance and multiple testing control

https://doi.org/10.5194/egusphere-2026-2680
Preprint. Discussion started: 28 July 2026

In the GLMM, this study employed a logit link function and examined the risk of overdispersion. Model fit was assessed for systematic bias by comparing residual bias with degrees of freedom and conducting simulated residual diagnostics. Discriminative ability of the binary model is characterized by AUC, while calibration ability is assessed using Brier score and calibration curves. Cross-validation grouped by events prevents spurious high performance due to overfitting. Given that slope position and depth may generate multiple testing issues across multiple metrics, the Benjamini-Hochberg method is employed to control the false discovery rate (FDR) when comparing the significance of slope position differences or lower-layer early response probabilities.

(4) Variable standardization and log transformation

To quantitatively examine the effects of slope position, depth, and their interaction on profile responses while controlling for differences in rainfall structure and background conditions between events, this study constructed mixed-effects models. Event e was treated as a random intercept, while slope position $j \in (F, M, T)$ and the normalized depth $zDepth_k$ at depth layer $k \in (10,20,30,40,50,60)$cm, along with their interaction term, were treated as core fixed effects. $AMC_{j,k,e}$, $P_{tot,e}$, and PI_e were simultaneously included as covariates. Continuous variables were uniformly standardized using z-scores to ensure comparability of coefficients across different units:

$$z(x) = \frac{x - mean(x)}{sd(x)}, \tag{26}$$

Where $zDepth_k = z(\mathrm{depth}_k)$, $zAMC_{j,k,e} = z(AMC_{j,k,e})$, $zPtot_e = z(P_{tot,e})$, $zPI_{15,e} = z(PI_{15,e})$. A logarithmic transformation is applied to the continuous response to mitigate skewness and heteroscedasticity. Let $\Delta\theta^{+}_{j,k,e}$ denote the maximum increment within the event window and $T_{i,j,k,e}$ denote the initial response delay. Then:

$$Y^{(\Delta\theta)}_{j,k,e} = ln\left(\Delta\theta^{+}_{j,k,e}\right), Y^{(T_i)}_{j,k,e} = ln\left(T_{i,j,k,e}\right), \tag{27}$$

The logarithmic model is fitted only to samples satisfying the response criterion ($R_{j,k,e} = 1$ and $T_i > 0$).

(5) Event-level mixed-effects model

For response occurrence, an event-level logistic mixed-effects model was used. Let $R_{j,k,e} \in (0,1)$ denote whether a significant response occurs at slope position j, k during event e, with threshold $\delta_\theta = 0.01$ (m^3 m^{-3}). Define $p_{j,k,e} = \Pr(R_{j,k,e} = 1)$, then:

$$logit\left(p_{j,k,e}\right) = ln\left(\frac{p_{j,k,e}}{1-p_{j,k,e}}\right) = \gamma_0 + \gamma_M I(j = M) + \gamma_T I(j = T) + \gamma_D zDepth_k + \gamma_{MD} I(j = M)\, zDepth_k + \gamma_{TD} I(j = T) zDepth_k + \gamma_{AMC} zAMC_{j,k,e} + \gamma_P zPtot_e + \gamma_{PI} zPI_e + b_e, b_e \sim \mathcal{N}(0, \sigma_b^2), \tag{28}$$

For a hierarchical linear mixed model of continuous response events, taking $\Delta\theta^{+}$ and T_i as an example:

$$ln\left(\Delta\theta^{+}_{j,k,e}\right) = \beta_0 + \beta_M I(j = M) + \beta_T I(j = T) + \beta_D zDepth_k + \beta_{MD} I(j = M)\, zDepth_k + \beta_{TD} I(j = T)\, zDepth_k + \beta_{AMC} zAMC_{j,k,e} + \beta_P zPtot_e + \beta_{PI} zPI_e + u_e + \varepsilon_{j,k,e}, u_e \sim \mathcal{N}(0, \sigma_u^2), \varepsilon_{j,k,e} \sim \mathcal{N}(0, \sigma^2), \tag{29}$$

$$ln\left(T_{i,j,k,e}\right) = \alpha_0 + \alpha_M I(j = M) + \alpha_T I(j = T) + \alpha_D zDepth_k + \alpha_{MD} I(j = M)\, zDepth_k + \alpha_{TD} I(j = T)\, zDepth_k + \alpha_{AMC} zAMC_{j,k,e} + \alpha_P zPtot_e + \alpha_{PI} zPI_e + v_e + \eta_{j,k,e}, v_e \sim \mathcal{N}(0, \sigma_v^2), \eta_{j,k,e} \sim \mathcal{N}\left(0, \sigma_\eta^2\right), \tag{30}$$

https://doi.org/10.5194/egusphere-2026-2680
Preprint. Discussion started: 28 July 2026

Other continuous indicators (such as T_{p2p}, V_{wf}, SI) are processed using the LMM form isomorphic to Eq. (29); interpretatively, fixing the fixed effects allows for the indexation of multiplicative effects, while indexing the logit model coefficients yields odds ratios (OR).

(6) Threshold and robustness tests

The core objective of threshold identification is to obtain interpretable trigger forms and quantify threshold uncertainty. In this study, using AMC and PI as core explanatory variables in segmented logistic regression, the inflection point τ describes the slope change in the trigger probability curve. Bootstrap resampling (1000 iterations) was employed to estimate the 95% confidence interval for τ. To prevent thresholds from being dominated by isolated outliers, resampling was conducted at the event scale. Each resampling iteration extracted an event set while preserving all slope-depth observations, aligning with the structure of the mixture model. Interpreted through the two-dimensional probability surface $Pr(DF = 1) = f(AMC, PI)$, this study employs cross-validation to minimize prediction error in smoothing parameter selection, ensuring the probability surface avoids unreasonable extrapolation in sparsely covered data regions. Interpretation of probability surface results is confined to the sample support range.

To validate that the method's conclusions are independent of specific manual settings, robustness tests were conducted on key criteria: Events were reconstructed and core metrics recalculated under IETD conditions of 4 h, 6 h, and 8 h; analyses were repeated with P_{tot} values of 10, 20, and 30 mm; recalculated T_i and DF discrimination under δ_θ conditions of 0.005, 0.01, and 0.02 m^3 m^{-3}; and recalculated lower-layer early response probability with tolerance expanded from Δt to $2\Delta t$ to test whether results are driven by temporal discretization.

4 Results

4.1 Hydrometeorological background and initial conditions

The 30 events selected from the 2024–2025 flood season (May–October) covered a wide range of hydrometeorological conditions (Fig. 2). The median P_{tot} was 31.75 mm (IQR: 16.50−55.00 mm), with a maximum value of 184.0 mm; the median duration D was 15.12 h (IQR: 7.50−26.31 h). The median PI_{15} was 4.00 mm 15 min^{-1}, with a maximum value reaching 24.5 mm 15 min^{-1}(Fig. 2a). The samples exhibited a wide range in peak intensity and duration, encompassing various combinations from short-duration high-intensity peaks to long-duration moderate-intensity peaks. Outlet flood responses varied strongly among events. The median Q_{peak} was 11.65 m^3 s^{-1} (IQR: 4.11–85.50 m^3 s^{-1}), with a maximum of 595.0 m^3 s^{-1}; The median maximum hydrograph rise rate $\left({}^{dQ}/_{dt}\right)_{max}$ was 2.90 m^3 s^{-1} h^{-1}(IQR：0.76-21.50 m^3 s^{-1} h^{-1}) with a maximum value of 119.0 m^3 s^{-1} h^{-1}(Fig. 2c).

$AMC_{j,k}(e)$ showed a clear position-depth structure before rainfall onset (Fig. 2b). In the upper monitored layers (10–30 cm), median AMC was generally higher at the mid-slope and slope-top positions than at the slope-foot position. At 10, 20, and 30 cm, the median values were 0.405, 0.414, and 0.403 m^3 m^{-3} at the mid-slope position; 0.417, 0.412, and 0.404 m^3 m^{-3} at the

https://doi.org/10.5194/egusphere-2026-2680
Preprint. Discussion started: 28 July 2026

slope-top position; and 0.303, 0.316, and 0.336 $m^3\ m^{-3}$ at the slope-foot position. In the lower monitored layers (40–60 cm), median AMC decreased with depth at the mid-slope and slope-top positions, with values of 0.382, 0.379, and 0.374 $m^3\ m^{-3}$ at the mid-slope position and 0.368, 0.353, and 0.331 $m^3\ m^{-3}$ at the slope-top position.

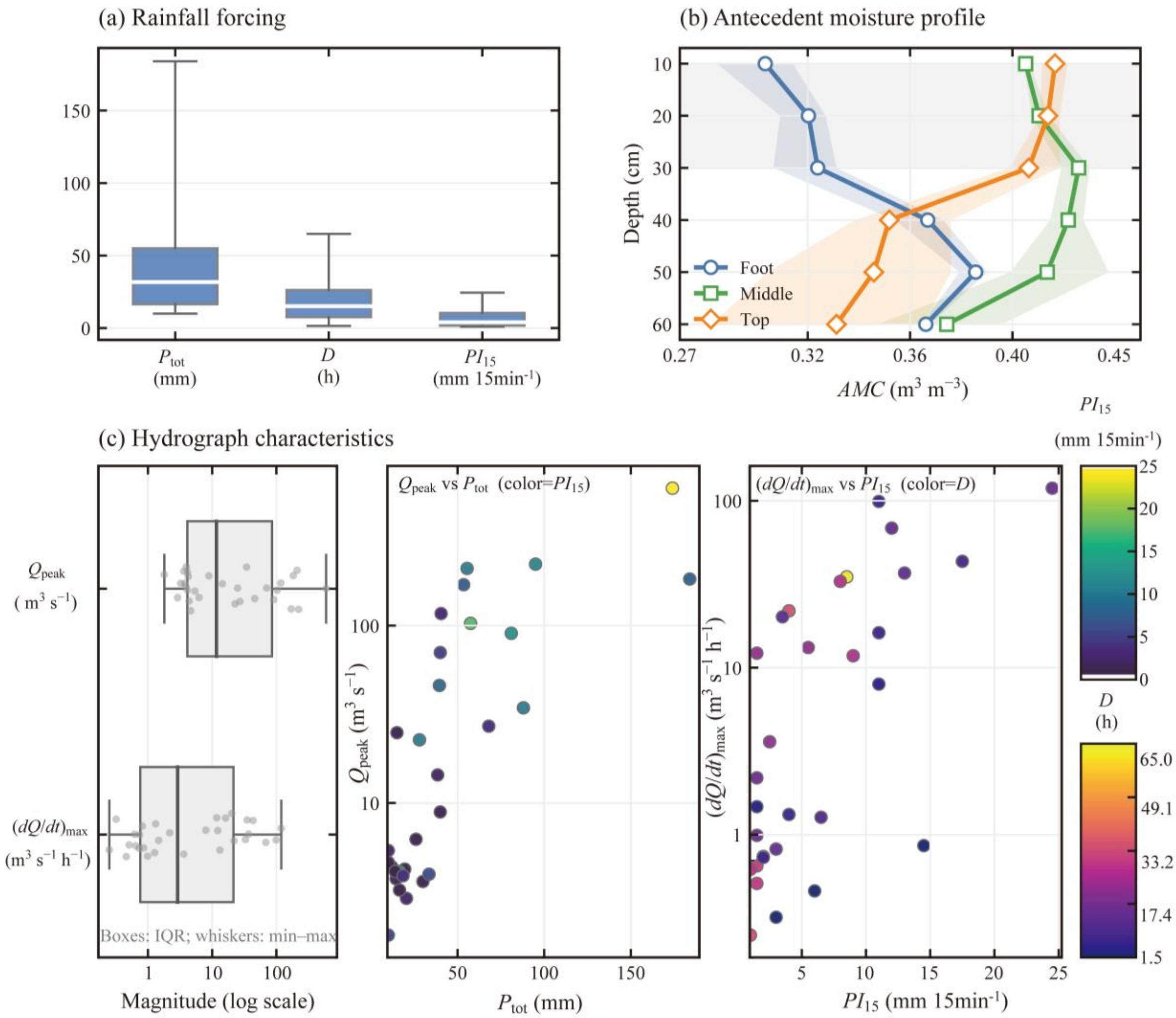

Figure.2. Hydrometeorological and Initial Conditions. (a) Distribution of rainfall indicators for the selected rainfall-runoff event, including: P_{tot}, D, PI_{15}. Boxes denote the interquartile range (IQR) with the median line. (b) Vertical stratification distribution of AMC at slope positions (foot, middle, and top). The x-axis shows AMC($m^3\ m^{-3}$) and the y-axis is depth (cm). Solid lines and symbols indicate medians, and shaded envelopes represent IQR. The grey background highlights the upper monitored layers (10–30 cm). (c) Event-scale flood characteristics and rainfall. Specifically: Distribution of $Q_{peak}$and $(dQ/dt)_{max}$(log-scaled), with scatter points representing event locations; Q_{peak}versus P_{tot} (point color indicates PI_{15}); $(dQ/dt)_{max}$versus PI_{15} (point color indicates D).

https://doi.org/10.5194/egusphere-2026-2680
Preprint. Discussion started: 28 July 2026

4.2 Position-depth differences in monitored-profile responses

4.2.1 Response occurrence and wetting magnitude across sensor depths

Using the response threshold $\delta_\theta = 0.01$(m³ m⁻³), the binary response indicator $R_{j,k}(e) \in 0,1$ showed clear differences among slope positions and sensor depths. The cross-event occurrence rate, $p_{R,j,k}$, defined in Eq. (18), describes how frequently each position-depth combination responded across the 30 events (Fig. 3a). The 10–40 cm layer at the foot responded in all events (p=1.00) ; however, the 50 cm layer showed a low response rate of 0.17, while the 60 cm layer increased to 0.83. The response rate in the mid-slope was lowest at the 30 cm layer (0.23), while the 60 cm layer approached full response (1.00). At the slope top, the 40–60 cm layer exhibited near-full response (≥0.97), but the 20 cm layer had a response rate of only 0.40.

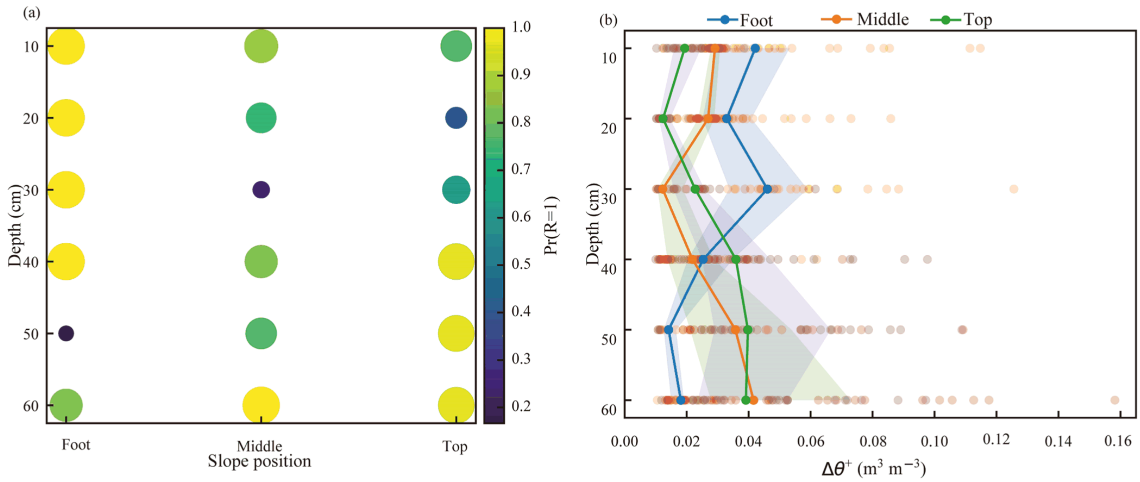

Figure.3. Response frequency and wetting magnitude across sensor depths. (a) Probability distribution of responses for each depth combination, where bubble color indicates $Pr(R = 1)$ and size scales proportionally with probability. (b) Stratigraphic profile of $\Delta\theta^{+}$($\mathrm{m^3\ m^{-3}}$), with shaded areas representing IQR and semi-transparent points overlaid with event values.

Regarding response amplification, the variation of the maximum increment $\Delta\theta^{+}_{j,k}(e)$ with depth exhibits significant slope−dependent characteristics (Fig. 3b). The median value of $\Delta\theta^{+}$ at the slope foot within the 10–30 cm layer ranges from 0.042 to 0.046 m³ m⁻³, significantly higher than that at the 60 cm layer (0.018 m³ m⁻³). At the slope-top position, wetting increments were larger in the lower monitored layers. Median values of $\Delta\theta^{+}$ at 40–60 cm being 0.036, 0.040, and 0.039 m³ m⁻³, respectively, markedly larger than those at 10–20 cm (0.017 and 0.009 m³ m⁻³). To describe both the range and duration of wetting within the event window, $\Delta\theta_{range}$ and A_θ were further calculated for the lower monitored layers (Fig. 4). A_θ for the lower monitored layers was positively correlated with D(Spearman ρ=0.50, p<0.01) and P_{tot} (ρ=0.46, p<0.01). Across slope positions, A_θ shows a consistent gradient of top > mid-slope > foot: The median (IQR) values for the foot, middle, and top were 0.150 (0.100–0.218), 0.295 (0.180–0.566), and 0.463 (0.254–0.689) m³ s⁻¹ h⁻¹, respectively; The median (IQR) of $\Delta\theta_{range}$ (mean 40–60 cm) was 0.055 (0.042–0.072) m³ m⁻³ at the foot, 0.078 (0.058–0.114) at the middle, and 0.109 (0.073–0.148) at the top (Fig. 4d).

https://doi.org/10.5194/egusphere-2026-2680
Preprint. Discussion started: 28 July 2026

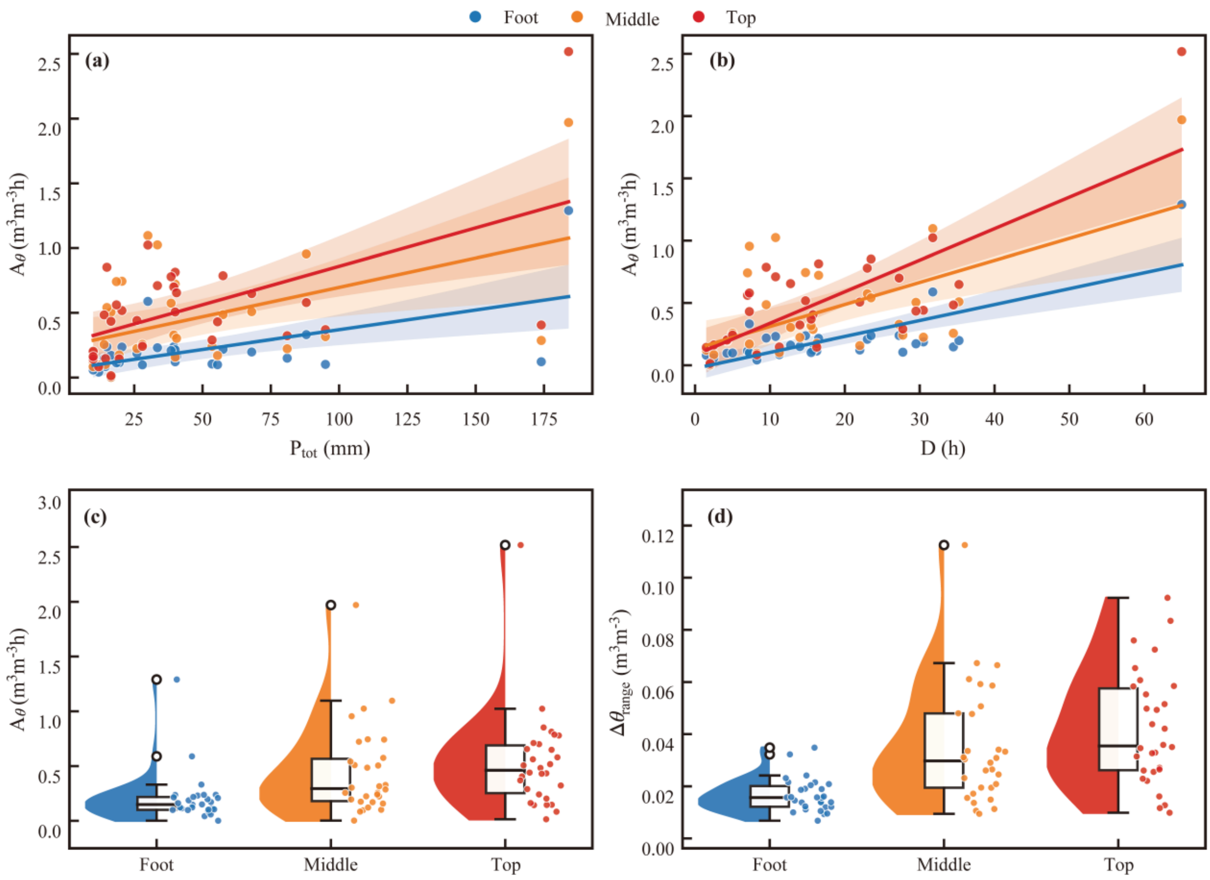

Figure.4. Event rainfall controls and slope-position differences in $A\theta$ and $\Delta\theta_{range}$ for the lower monitored layers. (a) Relationships between $A\theta$(40–60 cm) and P_{tot}; (b) Relationships between $A\theta$(40–60 cm) and D. Points represent events and are colored by slope position; solid lines indicate fitted trends with uncertainty bands. (c) Distributions of $A\theta$(40–60 cm) across slope positions. (d) Distributions of $\Delta\theta_{range}$(40–60 cm) across slope positions. Boxes show medians and IQRs with event points overlaid.

4.2.2 Mixed-effects results for response occurrence and wetting magnitude

To statistically account for event occurrence and magnitude differences under event heterogeneity, event-level mixed models (random intercept: event) were established. The logit mixed model for response occurrence probability R (n=540, 30 events) yielded the following results after controlling for $zAMC$、zP_{tot}、zPI_{15}(Fig. 5a): slope position effects relative to the foot were $\gamma_M = 1.384$(OR=3.991, $p < 0.0001$) for mid-slope and $\gamma_T = 0.738$(OR=2.092, $p = 0.0005$) for top. The main effect of depth was $\gamma_D = -0.967$ (OR=0.380, p<0.0001), with interaction terms $M \times zDepth = 1.354$ ($p < 0.0001$) and $T \times zDepth = 0.956$($p < 0.0001$). Among the covariates, $zAMC$ had a negative effect on response occurrence (OR=0.105), zP_{tot} had a positive effect (OR=1.733), while zPI_{15} did not reach significance.

https://doi.org/10.5194/egusphere-2026-2680
Preprint. Discussion started: 28 July 2026

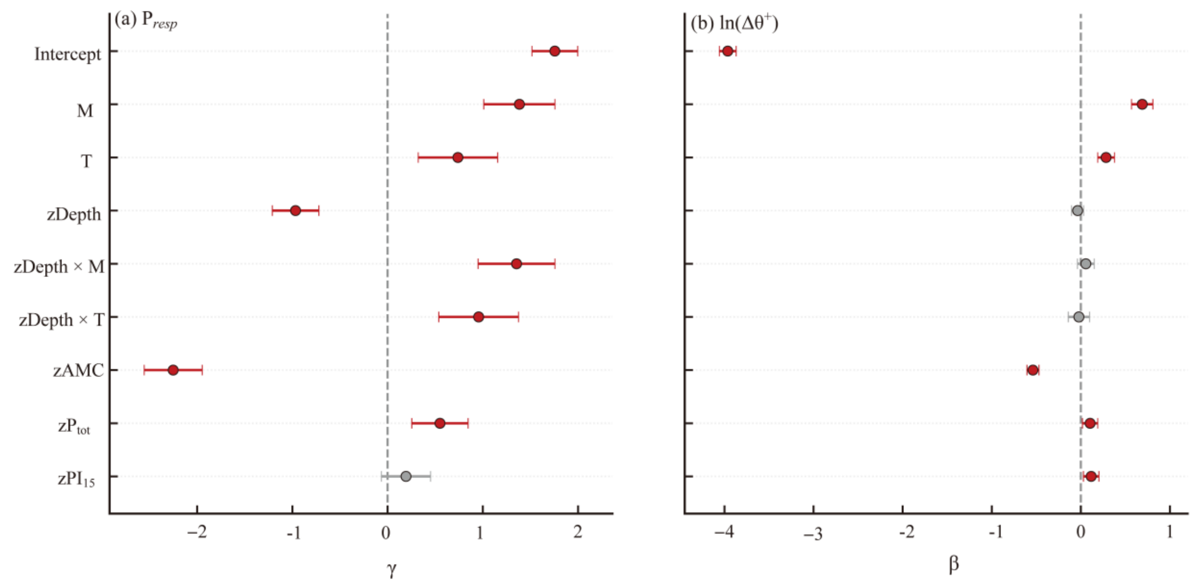

Figure.5. Quantitative attribution of profile response drivers based on mixed-effects models. (a) Fixed-effect estimates from the event-level logistic mixed-effects model for response occurrence P_{resp}; (b) fixed-effect estimates from the event-level linear mixed-effects model for response magnitude ln $(\Delta\theta^{+})$(. Predictors are listed on the y-axis; dots indicate coefficient estimates and horizontal bars denote 95% confidence intervals (CIs). The vertical dashed line marks the null effect ($\gamma = 0$ or $\beta = 0$); predictors whose CIs do not overlap zero are highlighted as significant (red), whereas non-significant predictors are shown in grey. Slope position is coded relative to the foot-slope reference level (M: middle; T: top). zDepth, zAMC, zP_{tot}, and $zPI_{15}$are z-standardized covariates. Both models include random intercepts for events (30 events; $n = 540$ for the logistic model and $n = 424$ for the linear model).

The linear mixed model for ln $(\Delta\theta^{+})$ (n=424, 30 events) after controlling for covariates within the same group (Fig.5b) yielded slope position effects relative to the foot of the slope at the middle and top of the slope, respectively, as $\beta_M = 0.689$ (exp $(\beta) = 1.992$, $p < 0.0001$) and $\beta_T = 0.283$(exp $(\beta) = 1.327$, $p < 0.0001$), respectively. Covariate estimates showed $zAMC$ had a significant negative effect (exp $(\beta) = 0.584$), while zP_{tot} and zPI_{15}both exhibited significant positive effects; neither the depth main effect nor its interaction with slope position reached statistical significance ($p > 0.05$).

4.3 Wetting timing and non-sequential responses

4.3.1 Response lag, peak-to-peak phase difference, and apparent wetting-front velocity

The profile distribution of $T_{i,j,k}(e)$ further reveals differences in infiltration advancement and sensor depths. The median T_i at the 10–40 cm layer near the slope foot clustered between 2.00 and 2.75 h; the median T_i at the 60 cm layer mid-slope was only 1.00 h, occurring earlier than its 10–20 cm layer (2.50 h and 3.00 h, respectively); at the top, the median T_i for the 40–50 cm layer was 2.50 and 2.25 h, respectively, and were not later than those in the upper monitored layers.

In most events, the peak soil moisture content lags behind the rainfall peak (primarily $T_{p2p,j,k}(e) > 0$), but its magnitude varies significantly with slope position and depth: medians across slope positions and depths cluster between 0.5 and 4.0 h, with

https://doi.org/10.5194/egusphere-2026-2680
Preprint. Discussion started: 28 July 2026

some lower monitored layers showing longer lags, for example 4.0 h at 40 cm at the slope-top position. Among all 540 samples (event × slope position × layer), the proportion of $T_{p2p} < 0$ was 0.035. Across all layer-slope combinations, the maximum negative phase difference occurrence rate was 0.143 (mid-slope at 30 cm). The distribution of V_{wf} was calculated for adjacent layers satisfying $T_{i,j,k+1} - T_{i,j,k} \geq \Delta t$. This distribution represents the propagation velocity of the sequence advancement subset. For adjacent pairs where both layers responded, $V_{wf} = \Delta z/\Delta T(\Delta z = 10$ cm). The number of valid adjacent pairs was 122 at the foot of the slope, 78 at the mid-slope, and 54 at the top. The median (IQR) of V_{wf} corresponds to the foot of the slope at 40.0 (20.0−40.0) cm h⁻¹, the mid-slope at 40.0 (4.0−40.0) cm h⁻¹, and the top at 10.0 (4.0−20.0) cm h⁻¹. At the event scale, T_{p2p} varied among slope positions and sensor depths, with its variation showing a parallel relationship with AMC and P_{tot}, as illustrated in Fig. 6.

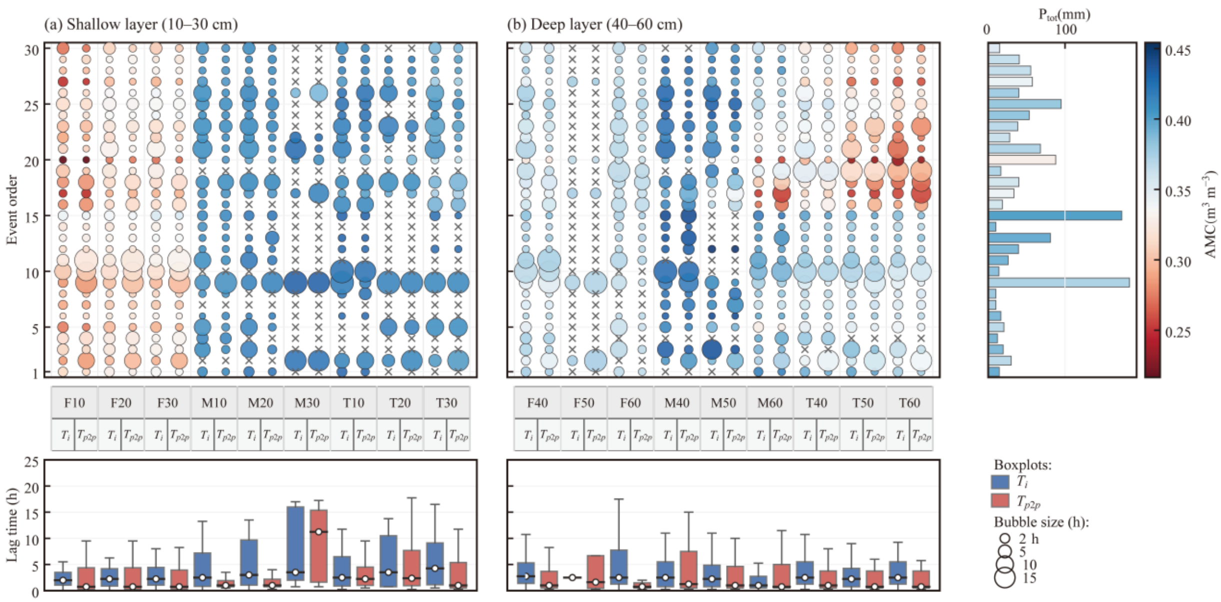

Figure.6. Event-scale distributions of the initial response lag and peak-to-peak phase shift across slope positions and depths, and their correspondence with antecedent wetness and event rainfall. Panels (a) and (b) summarize the upper monitored layers (10–30 cm) and lower monitored layers (40–60 cm), respectively, for three slope positions (F: foot; M: middle; T: top). Two adjacent columns are shown: T_i(initial lag; left) and T_{p2p}(peak-to-peak phase shift; right), as indicated by the grey header strip between the bubble matrix and the boxplots. The bubble matrix displays 30 rainfall events (y-axis: event order), where bubble size denotes the magnitude of the lag/phase shift (h) and bubble color denotes antecedent wetness (AMC, volumetric water content, m^3 m^{-3}; red–blue diverging scale). Events without a detectable response or with non-computable metrics are marked by "×". The right-hand bar chart reports total event rainfall P_{tot}(mm), with bar color mapped to event-mean AMC for direct comparison with profile-response timing. Bottom boxplots summarize the distributions of T_i(blue) and T_{p2p}(red) (median, interquartile range, and whiskers). To prevent a single extreme value from dominating the visualization, exceptionally large lag/phase-shift values were excluded from the boxplots only for F50 (foot-slope, 50 cm), while all other sensors were left untruncated.

https://doi.org/10.5194/egusphere-2026-2680
Preprint. Discussion started: 28 July 2026

4.3.2 Response occurrence, non-sequential occurrence, and timing metrics

According to the *DF* criterion, defined as a lower monitored layer responding at least one sampling step (Δt=0.25 h in advance),) earlier than an upper monitored layer, the DF occurrence rate was 0.77 at both the mid-slope and slope-top positions, but only 0.07 at the slope-foot position. Furthermore, $p_{NonSeq,j}$ values were 0.93 at the slope foot, 0.87 at the mid-slope, and 0.97 at the slope top. *SI* was higher in most events at the slope foot, while the median (IQR) *SI* values at the mid-slope and top were 0.40 (0.40–0.80) and 0.40 (0.25–0.60), respectively.

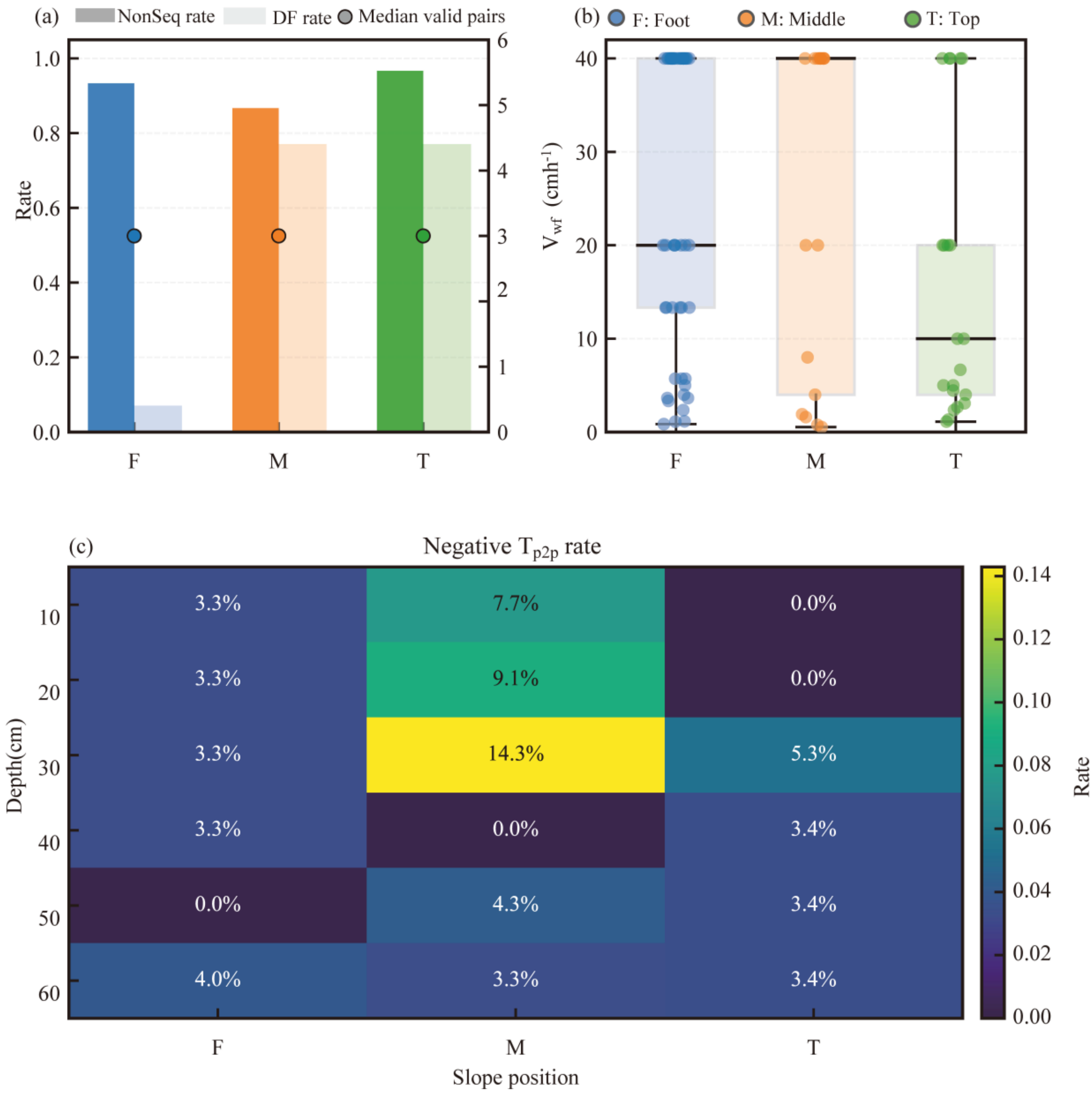

https://doi.org/10.5194/egusphere-2026-2680
Preprint. Discussion started: 28 July 2026

Figere.7. Diagnostics of non-sequential wetting and lower-layer early response (DF) across slope positions. (a) Event-level occurrence rates of non-sequential responses (NonSeq) and lower-layer early responses (DF) for each slope position. DF is identified when a lower monitored layer responds earlier than an upper monitored layer by at least one sampling step ($\Delta t = 0.25$ h). Circles denote the median number of valid adjacent-depth pairs ($\Delta z = 10$ cm) per event used for computing V_{wf}. (b) Distributions of wetting-front velocity V_{wf} computed from adjacent depth pairs only when sequential propagation holds $(T_{i,k+1} - T_{i,k} \geq \Delta t)$:$V_{wf} = \frac{\Delta z}{T_{i,k+1}-T_{i,k}}$(cm h^{-1}). Boxplots show medians and interquartile ranges; points represent individual valid pairs. (c) Heatmap of the occurrence rate of negative peak-to-peak phase shifts ($T_{p2p} < 0$) across depths and slope positions, where$T_{p2p} = T_{p,k+1} - T_{p,k}$. Negative values indicate that peak wetting in a lower monitored layer occurred before peak wetting in the layer above. Such timing does not follow a simple sequential downward wetting pattern F/M/T denote foot/middle/top positions, respectively.

4.3.3 Mixed-effects model for response lag and robustness

A hierarchical linear mixed model was established for ln (T_i) (random intercept: event; n=412, 30 events). Results indicate that the time lag at mid−slope is significantly shorter relative to foot ($\alpha_M = -0.370$, exp $(\alpha) = 0.691$, $p < 0.0001$), and the mid-slope × depth interaction term was significantly negative ($\alpha_{MD} = -0.249$, exp $(\alpha_{MD}) = 0.78$). The main effect of slope-top and its interaction with depth did not reach statistical significance. Among covariates, peak rainfall intensity significantly shortened T_i ($\alpha_{PI} = -0.823$, exp $(\alpha_{PI}) = 0.44$); whereas $zPtot$ and $zAMC$ exhibited positive effects.

Table 2 Event-level linear mixed model for response latency ln (T_i) (random intercept: event; n=412, 30 events)

Fixed effect term	β	95% CI	exp (β)	exp (CI_{low})	exp (CI_{high})	p
Intercept	1.028	[0.709,1.346]	2.795	2.032	3.843	<0.0001
M	-0.370	[-0.533,-0.208]	0.691	0.587	0.812	<0.0001
T	0.004	[-0.119,0.127]	1.004	0.888	1.136	0.945
$zDepth$	0.039	[-0.051,0.130]	1.040	0.950	1.139	0.393
M×$zDepth$	-0.249	[-0.376,-0.122]	0.780	0.687	0.885	0.0001
T×$zDepth$	0.042	[-0.120,0.204]	1.043	0.887	1.226	0.615
$zAMC$	0.303	[0.210,0.397]	1.354	1.234	1.487	<0.0001
$zPtot$	0.570	[0.167,0.973]	1.769	1.182	2.646	0.006
zPI	-0.823	[-1.227,-0.419]	0.439	0.293	0.658	<0.0001

Note: Random intercept variance $\sigma_v^2 = 0.7186$(SD=0.848); Residual variance $\sigma_\eta^2 = 0.1927$(SD=0.439); Explained variance $R_m^2 = 0.339, R_c^2 = 0.860$.

To assess the robustness of conclusions to parameter variations, this study recalculated all metrics while maintaining the final set of 30 events by altering the response threshold $\delta\theta$ (0.005–0.02 m³ m⁻³), sequential discrimination tolerance Δt (15–30 min), and IETD (4–8 h). Results indicate: When IETD was adjusted from 6 h to 4 h, the maximum change in response rate p_R across slope positions and depths did not exceed 0.067; slope-position differences in DF remained consistent (mid-slope/top still significantly higher than foot), with variation not exceeding 0.067; and NonSeq variation did not exceed 0.033. When the tolerance was extended from 15 min to 30 min, DF at mid-slope and top decreased by 0.167 and 0.267, respectively, but the

https://doi.org/10.5194/egusphere-2026-2680
Preprint. Discussion started: 28 July 2026

conclusion that mid-slope/top values remained significantly higher than foot values remained unchanged. When $\delta\theta$ was increased to 0.02 m³ m⁻³, DF decreased significantly at the top (–0.333), indicating sensitivity to discernible humidification levels. These tests support the use of $\delta\theta = 0.01$ m³ m⁻³ as the reference response threshold for balancing noise suppression and response detectability.

4.4 State-forcing thresholds for response occurrence and lower-layer early response

Given that stable thresholds are difficult to identify for layers with response rates close to 0 or 1, this study confined threshold analysis to layers with lower occurrence rates but still exhibiting 0/1 variation (slope-top 20 cm and mid-slope 30 cm). For trigger identification at $R = 1$, segmented logistic regression was employed to construct univariate inflection points for AMC or PI_{15}. Bootstrap resampling provided uncertainty intervals for thresholds, while 5-fold cross-validation quantified discrimination ability (AUC) and probability calibration (Brier score). Threshold estimates and model performance are summarized in the table.

Table 3 Threshold Estimation, Cross-Validation Performance, and Collinearity Diagnosis

Target Event	Subset	Segmented Variable	τ	95%CI	AUC_{cv}	$Brier_{cv}$	max VIF
R=1	T–20 cm	AMC	0.384	0.353-0.384	0.817	0.171	2.63
R=1	T–20 cm	PI_{15}	1.50	1.50-11.73	0.739	0.221	3100.73
R=1	M–30 cm	AMC	0.406	0.380-0.411	0.755	0.172	2.67
R=1	M–30 cm	PI_{15}	11.73	3.41-11.73	0.610	0.185	5.37
DF=1	Mid-slope position	AMC	0.400	0.364-0.400	0.740	0.167	2.78
DF=1	Slope-top position	PI_{15}	8.59	1.50-9.91	0.755	0.195	10.60
DF=1	Mid-slope position	AMC	0.380	0.380-0.422	0.490	0.195	4.89
DF=1	Mid-slope position	PI_{15}	2.14	1.50-11.73	0.750	0.133	697.82
DF=1	Bivariate probability surface (T)	AMC+PI	—	—	0.870	0.172	—
DF=1	Bivariate probability surface (M)	AMC+PI	—	—	0.845	0.191	—

For response occurrence, the segmented AMC model identified a threshold of $\tau_{AMC} = 0.384$ m³ m⁻³at the slope-top 20 cm sensor (95%CI: 0.353–0.384), and $\tau_{AMC} = 0.406$ m³ m⁻³ at the mid-slope 30 cm sensor (95%CI: 0.380–0.411); cross-validation AUC values were 0.817 and 0.755, respectively, with a Brier score of approximately 0.17. In contrast, using PI_{15}as a piecewise variable resulted in greater threshold uncertainty and lower AUC values, particularly for the 30 cm mid–slope region where AUC_{cv} was only 0.610.

For DF=1, threshold behaviour was evident at the slope-top and mid-slope positions, although the uncertainty was larger than for response occurrence. At the slope-top position, the segmented threshold for AMC is $\tau_{AMC} = 0.400$ m³ m⁻³ (95% CI: 0.364–

https://doi.org/10.5194/egusphere-2026-2680
Preprint. Discussion started: 28 July 2026

0.400), corresponding to AUC$_{cv}$=0.740; the segmented threshold for PI_{15} was τ_{PI} = 8.59 mm 15 min^{-1} (95% CI: 1.50–9.91), corresponding to AUC$_{cv}$=0.755. The threshold identification of DF in the slope region exhibited stronger event heterogeneity: the AMC segmented model showed weaker discrimination ability (AUC$_{cv}$=0.490), while the PI_{15} segmented model, despite having a higher AUC$_{cv}$=0.750 , exhibited significantly amplified collinearity in its design matrix (max VIF reaching 10^2–10^3 magnitude), necessitating comprehensive interpretation integrating bootstrap intervals, cross-validation, and two-dimensional probability surface results.

To characterize the continuous variation of Pr $(DF = 1)$ in the AMC and PI_{15} two-dimensional space and overcome the limitations of single-threshold interpretation, a two-dimensional probability surface model was further constructed. Its generalization performance was evaluated using 5-fold cross-validation. The two-dimensional probability surface demonstrates high discrimination capability at the slope top (AUC$_{cv}$=0.870, Brier$_{cv}$=0.172), and also achieves a good level in the mid-slope (AUC$_{cv}$=0.845, Brier$_{cv}$=0.191). As a supporting sensitivity check, the GBDT partial dependence curves and variable-importance results were broadly consistent with the segmented and probability-surface analyses. In the R=1 discrimination between the 20 cm slope top and 30 cm mid-slope, the relative contributions of AMC were 0.765 and 0.690, respectively, both higher than PI_{15} （(0.235 and 0.310, respectively), while event-scale hydrological variables (e.g., P_{tot}) showed marginal contributions.

https://doi.org/10.5194/egusphere-2026-2680
Preprint. Discussion started: 28 July 2026

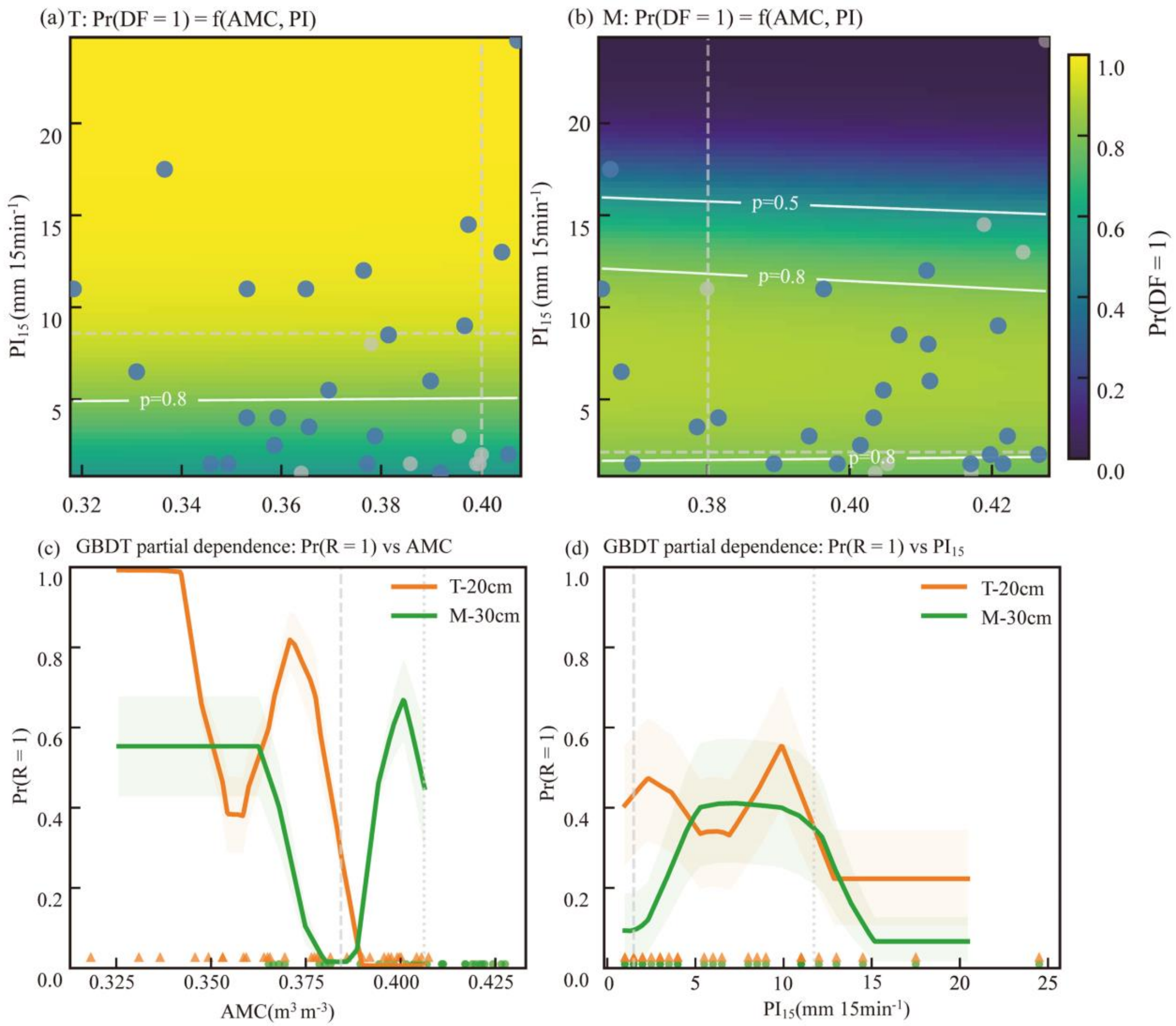

Figure.8.Joint characterization of DF/response occurrence using 2-D conditional probability surfaces and GBDT partial dependence plots. (a–b) Two-dimensional conditional probability surfaces for the slope-top (T) and mid-slope (M) positions. Background shading indicates $\Pr(DF = 1 \mid AMC, PI_{15})$ where AMC is antecedent wetness (m^3 m^{-3}) and PI_{15} is the 15-min peak rainfall intensity (mm 15 min^{-1}). Grey dots denote observed event samples in the $AMC - PI_{15}$ space. Light-grey vertical/horizontal dashed lines mark the threshold locations (τ_{AMC}, τ_{PI}), and white curves indicate probability isolines (e.g., $p = 0.5$, $p = 0.8$). (c–d) GBDT partial dependence plots (PDPs) showing the marginal effects of AMC and PI_{15} on Pr ($R = 1$). Orange curves represent T–20 cm and green curves represent M–30 cm; shaded bands denote bootstrap 95% confidence intervals; light-grey vertical lines indicate the corresponding threshold locations (τ). Axis markers show the empirical distribution of event samples (T: triangles; M: dots).

https://doi.org/10.5194/egusphere-2026-2680
Preprint. Discussion started: 28 July 2026

4.5 Associations between monitored-profile responses and outlet flood characteristics

At the event scale, outlet flood metrics were first compared with rainfall descriptors. Q_{peak} shows significant positive correlations with both P_{tot} and PI_{15} (Spearman ρ values of 0.786 and 0.585, respectively); $(dQ/dt)_{\max}$ exhibited even stronger correlations with both variables (ρ = 0.850 and 0.683).

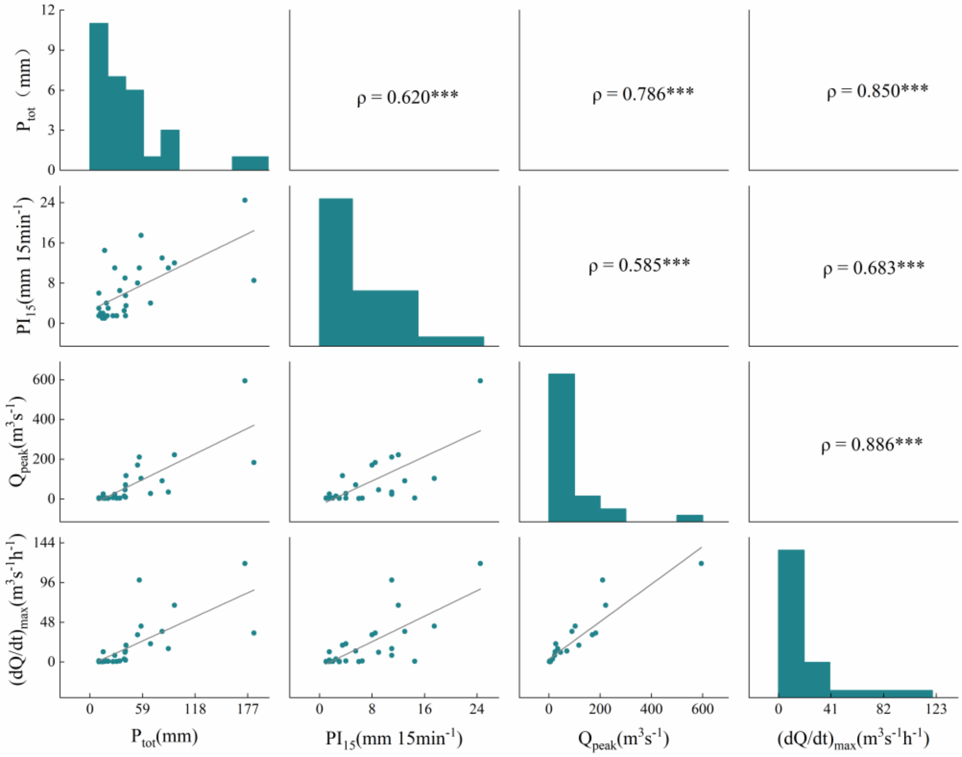

Figure.9. Rank correlations between rainfall and flood response. Spearman rank correlations between rainfall descriptors and outlet flood responses across the 30 events: (a) Q_{peak}vs. P_{tot}, (b) Q_{peak}vs. PI_{15}, (c) $(dQ/dt)_{max}$vs. P_{tot}, and (d) $(dQ/dt)_{max}$vs. PI_{15}. Each dot denotes one event. Annotations report Spearman's $\rho$with significance levels (* p < 0.05; ** p < 0.01; *** p < 0.001).

After controlling for multiple testing using the BH–FDR procedure, several monitored-profile metrics remained significantly associated with outlet flood metrics. Taking the slope-position event mean $\Delta\bar{\theta}^{+}{}_{j}(e)$ as an example, the correlation coefficient between $\Delta\bar{\theta}^{+}{}_{top}$ and Q_{peak} was ρ=0.669 (p<0.001); and with $(dQ/dt)_{max}$ at ρ=0.774 (p<0.001). Mid-slope correlations were weaker (0.371 and 0.543, respectively), while slope foot correlations were even weaker (0.307 and 0.299). Using mean $\Delta\theta^{+}$ in the lower monitored layers (40–60 cm) at the slope-top position as an indicator, the correlation with $(dQ/dt)_{\max}$ was ρ=0.793 (p<0.001), and with Q_{peak} was ρ=0.653 (p<0.001). All 12 correlations remained significant after BH–FDR correction (q<0.01). In contrast, the correlation between the average foot-of-slope humidification and peak flood indicators was very weak. Timing-based response metrics also showed directional differences between events with and without DF, although these differences should be interpreted as event-scale associations rather than direct causal links. Taking the top DF as an example,

https://doi.org/10.5194/egusphere-2026-2680
Preprint. Discussion started: 28 July 2026

the median Q_{peak} for events with DF=1 was 24.90 m³ s⁻¹, while it was 4.63 m³ s⁻¹ for DF=0. For mid-slope DF=1 and DF=0, the median Q_{peak} values were 14.40 and 4.63 m³ s⁻¹, respectively.

5 Discussions

This study used 15 min soil moisture observations from three slope positions and six sensor depths within the upper 60 cm soil profile to examine event-scale wetting patterns across 30 rainfall-runoff events. The results show that wetting responses were organized by both slope position and sensor depth, but not as a simple monotonic change with depth. The upper monitored layers at the slope foot responded frequently, whereas selected lower monitored layers at the mid-slope and slope-top positions showed larger wetting increments and more frequent early or near-synchronous responses. These lower-layer wetting signals at the slope-top position were also associated with outlet peak discharge and hydrograph rise rate at the event scale. The discussion therefore focuses on four issues: position-depth differences in near-surface wetting, the interpretation of non-sequential wetting and lower-layer early response, state-forcing thresholds, and the extent to which monitored-profile wetting signals can help explain flood-peak variability.

5.1 Position-depth differences in event-scale wetting responses

Slope position and sensor depth jointly shaped the event-scale wetting response within the monitored profile. The main pattern was not a simple upper-to-lower attenuation, but a set of position-depth response combinations. At the occurrence level, the profile structure of p_R reveals stable responsive and unresponsive layers at different slope positions, and this structure remains consistent in both descriptive distributions and statistical models of occurrence probability (Fig. 3a, Fig. 5a). This implies that slope position carries independent process significance for response: it modulates not only through moisture background effects but also likely alters layer responsiveness via differences in soil structure and redistribution pathways. The observed pattern, frequent responses in the upper monitored layers at the slope foot and stronger lower-layer responses at the slope-top position, is consistent with recent high-frequency soil moisture studies showing that response type varies with slope position and sensor depth. Lee and Kim (2021) demonstrated through event typology that distinct combinations of slope position and depth response serve as observable fingerprints for dominant slope processes (such as near-surface lateral flow, matrix infiltration, and preferential flow connectivity). This is relevant here because the main signal was not the mean moisture state alone, but the combination of response occurrence, wetting magnitude, and timing. Furthermore, Han et al. (2021) emphasized that topographic undulations systematically govern the spatial distribution and redistribution of water content during wet-dry transitions, leading to differentiated recharge pathways across different terrain sections during the same event. Together with the present results, these studies suggest that slope position affects near-surface storage and redistribution conditions, rather than simply changing the amount of wetting at each depth.

At the magnitude level, $\Delta\theta^{+}$ describes the maximum wetting response relative to antecedent moisture, but it does not capture how long the wetting departure persisted within the event window. A_{θ} and $\Delta\theta_{\mathrm{range}}$ therefore provide complementary information on sustained wetting and within-event variability in the lower monitored layers (40–60 cm). Their differences

https://doi.org/10.5194/egusphere-2026-2680
Preprint. Discussion started: 28 July 2026

among slope positions show that lower-layer wetting was stronger at the slope-top and mid-slope positions than at the slope foot (Fig. 4c–d). Together, these findings indicate that the deep-seated zone on the uphill slope exhibits stronger reservoir fluid fluctuations and more pronounced sustained recharge signals within the event window. The mixed-effects model for $\ln(\Delta\theta^{+})$ supports this interpretation: slope-position effects remained clear after accounting for event-level random effects, rainfall input, and antecedent moisture, whereas depth effects were not consistently significant for wetting magnitude (Fig.5b). The magnitude differences are therefore more reasonably interpreted as differences in near-surface storage and redistribution among slope positions, rather than as a simple attenuation of vertical infiltration with depth. Similar insights are common in studies emphasizing that response combinations and dynamic structures are more critical for process inversion: soil moisture response to rainfall is not simply a top-down progression of wetting fronts, but rather a heterogeneous infiltration and redistribution process shaped by soil structural pores, local convergence, and profile connectivity (Kan et al., 2020; Graf et al., 2021). Singh et al. (2021) demonstrated that identifying characteristics such as response and connectivity based on event-scale soil moisture time series is an effective approach to distinguishing infiltration mechanisms and flow pathways. Crucially, the consistency between temporal indicators and spatial variations is not statistically coincidental. The timing and magnitude results should therefore be read together. Some lower monitored layers at the mid-slope and slope-top positions had relatively large wetting magnitudes, even when their timing did not follow a simple sequential pattern. This indicates that wetting within the monitored profile was not always controlled by slow layer-by-layer propagation.

5.2 Non-sequential wetting and lower-layer early response

Wetting magnitude alone is not sufficient to distinguish sequential wetting from non-sequential timing within the monitored profile. The timing metrics T_i, T_{p2p}, SI, DF, and NonSeq were therefore used to describe the order and phase of wetting responses.. The profile distribution of T_i hat lower monitored layers at the mid-slope and slope-top positions sometimes responded no later than the upper monitored layers (Fig.6). The mixed-effects model for $\ln(T_i)$ also showed a significant interaction between mid-slope position and depth, while higher PI_{15} was associated with shorter response lags. This suggests that high short-duration rainfall intensity can reduce timing differences among monitored layers during some events. T_{p2p} provides a related timing signal. Although peak soil moisture generally lagged behind peak rainfall intensity, negative or near-synchronous phase differences occurred at some position-depth combinations (Figs. 6 and 7c). This signal defies explanation by simple layer-by-layer progression and aligns better with scenarios where deep-layer peaks are influenced by bypass recharge or lateral input (Pinos et al., 2023). This is consistent with the higher DF occurrence at the mid-slope and slope-top positions. NonSeq, DF, and SI should be interpreted as timing diagnostics rather than direct process labels (Fig.7a). Given that NonSeq's discrimination is fundamentally a tolerance classification for discrete sequences, its physical meaning must be interpreted in conjunction with DF and SI typologies: NonSeq occurring together with DF provides stronger evidence of lower-layer early response, whereas NonSeq caused by weak or missing responses in intermediate layers does not necessarily indicate rapid preferential wetting. DF is therefore used as the main event label for lower-layer early response, whereas NonSeq and SI provide supporting information on the degree of departure from sequential wetting (Fig.7a). This interpretation is consistent with high-frequency monitoring studies showing that soil structure and profile organization can affect preferential wetting and rapid responses at depth. For example, Zhang et al. (2025) showed that soil thickness modulated preferential flow occurrence and depth-dependent wetting response. This supports the use of response timing as a useful descriptor of profile-scale wetting organization, provided that the limits of sensor depth and spatial representativeness are made explicit. From a broader perspective of transferability, Li et al. (2025) further indicate in their cross-ecosystem study that the triggering of priority flows exhibits an inductive threshold structure, with thresholds jointly constrained by climate and soil structure.

Finally, V_{wf} represents adjacent layer pairs that maintain sequence progression (Fig.7b), and its interpretive boundaries require clarification: the calculation of V_{wf} itself relies on adjacent layers uniformly responding and satisfying sequence conditions. Therefore, it is better suited to characterize the propagation features of sequence-progression subsets rather than inferring the overall process speed of DF- and NonSeq-dominated events. Interpreting V_{wf} in conjunction with DF and NonSeq avoids over-reliance on a single metric to represent complex processes.

5.3 State-forcing thresholds for lower-layer early response

The threshold results support a state-forcing interpretation of near-surface wetting organization. In steep catchments, runoff generation and preferential wetting often respond nonlinearly to the combined effects of antecedent storage and rainfall forcing. Conversely, under drier conditions or when structural connectivity is absent, even substantial cumulative rainfall may primarily remain confined to shallow storage and local redistribution phases. Previous studies provide the process context for this interpretation. Nanda and Safeeq (2023) showed that runoff thresholds and flow-path types vary with event storage and rainfall characteristics. Ran et al. (2022) and Fischer-Bedtke et al. (2023) also showed that antecedent soil moisture and rainfall forcing can have comparable importance in event runoff generation, with their relative roles depending on catchment or hillslope conditions. In event-driven flood generation, prior soil moisture conditions and rainfall input often hold comparable importance, with their relative contributions modulated by basin/slope characteristics. For the present data, the more relevant question is not whether a single universal threshold exists, but whether lower-layer early response within the monitored profile becomes more likely under particular combinations of antecedent moisture and short-duration rainfall intensity.

The threshold analysis indicates that response occurrence and DF are better explained by state-forcing combinations than by rainfall intensity alone. For the low-occurrence sensors used in the threshold analysis, AMC-related breakpoints had clearer cross-validation performance than some PI_{15}-based thresholds. This suggests that antecedent moisture describes how close the monitored profile is to a response threshold, whereas short-duration rainfall intensity acts as event forcing that can trigger a detectable response once the profile is sufficiently wet. The presence of wet events without DF is also informative. It indicates that lower-layer early response depends on both antecedent state and effective rainfall forcing, rather than on pre-event wetness alone.

https://doi.org/10.5194/egusphere-2026-2680
Preprint. Discussion started: 28 July 2026

For DF, the two-dimensional probability surface provides a more suitable description than a single threshold. $Pr(DF = 1 \mid AMC, PI_{15})$ increased most clearly where high antecedent moisture coincided with high short-duration rainfall intensity (Fig. 8a–b). The GBDT results were used only as a supporting sensitivity check and were broadly consistent with this state-forcing interpretation (Fig. 8c–d). Thus, overreliance on numerical interpretations of single τ_{AMC} or τ_{PI} values should be avoided. Marcotte et al. (2024) demonstrated that connectivity can undergo sudden enhancement during heavy rainfall periods, leading to the expansion of fast-flow pathways; Uhlemann et al. (2024) emphasized that state-dependent connectivity gating manifests as probabilistic transitions and threshold-like behavior at the event scale. The threshold results should therefore be interpreted as empirical transition ranges within the present event sample. They support a state-forcing control on lower-layer early response within the monitored near-surface profile, but they do not define fixed physical thresholds for deep groundwater connectivity.

5.4 Monitored-profile wetting signals and outlet flood response

The event-scale comparison between monitored-profile responses and outlet flood metrics shows that rainfall remained the main control on peak magnitude and hydrograph rise rate (Fig. 9), while several soil moisture response metrics provided additional process information. In particular, $\Delta\theta^+$, $\Delta\theta_{range}$, A_θ and timing labels such as DF, NonSeq, and SI showed clearer associations with Q_{peak} and $(dQ/dt)_{max}$ at the slope-top and mid-slope positions than at the slope foot. These results suggest that lower-layer wetting signals at upslope positions may indicate a wetter and more responsive hillslope state during some events. Such a state may coincide with larger effective contributing areas or faster runoff transmission, but the present observations do not identify the actual flow paths. Crompton et al. (2023) on patch connectivity in arid slopes indicate that local connectivity structures can scale up to alter overall slope runoff response and determine which regional indicators explain slope output. Dralle et al. (2023) similarly showed that storage-discharge relationships can become steeper when subsurface storage and flow pathways are more effectively connected. Similarly, studies emphasizing the application of preferential flow and connectivity structures in flood response, as well as those constraining rainfall-runoff conversion with soil moisture dynamics, provide external consistency evidence (Li et al., 2023; Kaffas et al., 2025).

The association between slope-top lower-layer wetting and outlet flood response should therefore be treated as an indicator relationship rather than direct causal attribution. Rainfall spatial variability, hillslope-channel routing, and the expansion of contributing areas all lie between the local sensor response and the outlet hydrograph. The lower-layer wetting signal at the slope-top position is best interpreted as evidence that the monitored profile had entered a wetter and more responsive state during some events. Groundwater levels, hydraulic gradients, tracer data, or geophysical observations would be needed to test the underlying flow paths.

https://doi.org/10.5194/egusphere-2026-2680
Preprint. Discussion started: 28 July 2026

5.5 Uncertainty

The conclusions of this study are based on one monitored hillslope line with three slope positions. Differences among slope positions may include effects of local soil structure, vegetation, and microtopography, so the inferred position effects should be transferred only with caution to similar terrain-soil settings. The 15 min sampling interval may also miss faster preferential wetting or short-lived redistribution, which adds uncertainty to T_i, T_{p2p}, NonSeq, and DF for individual events. Robustness tests were conducted by recalculating key metrics under varying IETD, $\delta\theta$, and DF tolerance settings to verify consistency in slope position comparisons and threshold structures. The robustness tests show that the main slope-position contrasts in DF and NonSeq were not removed by reasonable changes in IETD, $\Delta\theta$, or timing tolerance, although exact phase differences for individual events remain sensitive to temporal resolution. Finally, coupling between channel confluence and source area connectivity persists from the slope profile process to the outlet peak flow. Thus, the correspondence between DF and NonSeq with peak flows should be interpreted as a process relationship rather than a single causal determinant. Future work should add parallel hillslope profiles, use higher-frequency soil moisture measurements, and include groundwater level, pore-water pressure, tracer, or geophysical observations where possible. These additions would help test whether the lower-layer early responses identified here correspond to specific subsurface flow paths beyond the monitored 0–60 cm profile.

6 Conclusions and future work

This study utilized 15-minute rainfall, outlet discharge, and soil moisture observations from three slope positions and six sensor depths within the upper 60 cm of the soil profile to examine event-scale wetting responses in the Ganwuli River basin. The analysis focused on whether monitored-profile wetting responses followed a simple upper-to-lower sequence, how these responses were related to antecedent moisture and rainfall forcing, and whether they were associated with outlet flood variability. The results do not provide direct evidence of deep groundwater flow paths. Instead, they demonstrate that lower-layer early response and non-sequential wetting within the monitored profile can serve as event-scale indicators of changing near-surface wetting organization. The main conclusions are as follows.

(1) The 30 rainfall-runoff events showed clear position-depth differences in wetting response within the monitored 0–60 cm soil profile. At the slope foot, sensors at 10–40 cm responded in all events. The 50 cm sensor responded to only 0.17 of the events. At mid-slope and slope-top, the lower layers (40–60 cm) exhibited more frequent responses and larger wetting increments than some upper layers. This pattern indicates that wetting response within the profile was influenced by both slope position and sensor depth, not depth alone.

(2) Antecedent moisture showed a distinct position-depth structure and affected the likelihood of detectable wetting responses. The threshold analysis suggests that lower-layer early response was more likely when higher antecedent moisture coincided with stronger short-duration rainfall intensity. This supports a state-forcing interpretation, in which antecedent moisture

https://doi.org/10.5194/egusphere-2026-2680
Preprint. Discussion started: 28 July 2026

describes the pre-event wetness state of the monitored profile, and PI_{15} acts as an event forcing. The results should be interpreted as changes in monitored-profile wetting organization, not as direct evidence of deep-layer connectivity or recharge.

(3) Lower-layer early response, denoted as DF, occurred much more often at the mid-slope and slope-top positions (both 0.767) than at the slope-foot position (0.067). NonSeq was also common across the three slope positions, with occurrence rates of 0.867–0.967. These two timing metrics describe different aspects of non-sequential wetting. DF identifies cases when a lower monitored layer responded earlier than an upper one. NonSeq also includes near-synchronous responses or non-monotonic timing between adjacent layers. DF is therefore used as the main event label for lower-layer early response. NonSeq and SI describe the broader degree of departure from a sequential upper-to-lower wetting pattern.

(4) Monitored-profile wetting metrics were associated with outlet flood variability, but these associations should not be interpreted as direct causal flow paths. The slope-top wetting magnitude showed a clear event-scale association with Q_{peak}, and lower-layer wetting at the slope-top position was also related to hydrograph rise rate. DF grouping further showed that events with DF = 1 had larger median Q_{peak} than events with DF = 0. These results suggest that lower-layer early response within the monitored profile can serve as an indicator of a wetter and more responsive hillslope state during some events.

(5) The threshold analysis showed that response occurrence and DF were better described by combinations of antecedent moisture and short-duration rainfall intensity than by rainfall forcing alone. The AMC-related thresholds were clearer than some PI_{15}-based thresholds for low-occurrence sensors, while the two-dimensional probability surface showed that DF became more likely when high antecedent moisture and high PI_{15} occurred together. These thresholds should be treated as empirical transition ranges within the present event sample, rather than as fixed physical constants or operational warning thresholds.

Future work should first test the spatial robustness of these results by adding parallel hillslope monitoring lines and by sampling a wider range of slope positions, soil depths, soil structures, and vegetation conditions. Independent information on soil thickness, weathered-bedrock structure, groundwater level, pore-water pressure, or tracer movement would be needed to test whether the lower-layer early responses identified here correspond to specific subsurface flow paths beyond the monitored 0–60 cm profile. A second direction is to test whether the event-scale state-forcing relationships identified from field observations can be transferred to larger spatial scales. Satellite soil moisture products may help describe basin-scale antecedent wetness, but their use for threshold identification should be evaluated against independent runoff and in situ soil moisture observations before being used in forecasting. Studies such as Ortenzi et al. (2025) show that satellite soil moisture can be useful for identifying runoff-related wetness thresholds, but the transfer from point-scale profile responses to satellite-scale antecedent wetness remains a separate source of uncertainty. Machine-learning tools may also be useful for screening large soil moisture datasets, but they should remain secondary to process-based interpretation and independent hydrological validation.

https://doi.org/10.5194/egusphere-2026-2680
Preprint. Discussion started: 28 July 2026

Code and data availability

No custom code was developed specifically for this study. The original hydrometeorological observations used in this study were provided by the local Hydrology Bureau and are subject to third-party administrative and licensing restrictions. The authors do not have permission to redistribute the raw station records. To support reproducibility, the processed event-scale datasets underlying the figures, tables, and main results of this paper, together with variable descriptions and metadata necessary to interpret them, are archived in Zenodo at **https://doi.org/10.5281/zenodo.18973096**. The repository record will be made publicly accessible upon final publication of the paper.

Supplement link

The link to the supplement will be included by Copernicus, if applicable.

Author contributions

Yi Ao: Conceptualization, Methodology, Investigation, Writing - original draft, Formal analysis. **Xiaorong Huang:** Software, Methodology, Writing - review & editing, Resources, Funding acquisition. **Yanjun Wang:** Writing - review & editing. **Yangwen Jia**: Conceptualization, Project administration, Resources, Funding acquisition. **Bibo Huang**: Provide data support.

Competing interests

The authors declare that they have no conflict of interest.

Acknowledgements

Thanks for the long-term support from Chengdu Hydrological and Water Resources Survey Center.

Financial support

This research has been supported by Science and Technology Projects of Xizang Autonomous Region, China (XZ202501ZY0004); The National Natural Science Foundation of China (52279030).

https://doi.org/10.5194/egusphere-2026-2680
Preprint. Discussion started: 28 July 2026

References

Cain, M. R., Woo, D. K., Kumar, P., Keefer, L., and Ward, A. S.: Antecedent Conditions Control Thresholds of Tile-Runoff Generation and Nitrogen Export in Intensively Managed Landscapes, Water Resour. Res., 58, e2021WR030507, https://doi.org/10.1029/2021WR030507, 2022.

Crompton, O., Katul, G., Lapides, D., and Thompson, S.: Hydrologic Connectivity and Patch-To-Hillslope Scale Relations in Dryland Ecosystems, GEOPHYSICAL RESEARCH LETTERS, 50, 10.1029/2022GL101801, 2023.

Dralle, D. N., Hahm, W. J., and Rempe, D. M.: Inferring Hillslope Groundwater Recharge Ratios From the Storage-Discharge Relation, Geophysical Research Letters, 50, e2023GL104255, https://doi.org/10.1029/2023GL104255, 2023.

Fischer-Bedtke, C., Metzger, J. C., Demir, G., Wutzler, T., and Hildebrandt, A.: Throughfall spatial patterns translate into spatial patterns of soil moisture dynamics – empirical evidence, Hydrol. Earth Syst. Sci., 27, 2899-2918, https://doi.org/10.5194/hess-27-2899-2023, 2023.

Graf, M., Arnault, J., Fersch, B., and Kunstmann, H.: Is the soil moisture precipitation feedback enhanced by heterogeneity and dry soils? A comparative study, Hydrological Processes, 35, e14332, https://doi.org/10.1002/hyp.14332, 2021.

Han, X., Liu, J., Srivastava, P., Mitra, S., and He, R.: Effects of critical zone structure on patterns of flow connectivity induced by rainstorms in a steep forested catchment, Journal of Hydrology, 587, 125032, https://doi.org/10.1016/j.jhydrol.2020.125032, 2020.

Han, X., Liu, J., Srivastava, P., Liu, H., Li, X., Shen, X., and Tan, H.: The Dominant Control of Relief on Soil Water Content Distribution During Wet-Dry Transitions in Headwaters, Water Resour. Res., 57, e2021WR029587, https://doi.org/10.1029/2021WR029587, 2021.

Kaffas, K., Murgia, I., Menapace, A., Macchioli Grande, M., Verdone, M., Dani, A., Manca di Villahermosa, F. S., Preti, F., Segura, C., Massari, C., Klaus, J., Borga, M., and Penna, D.: Controls on preferential flow and its role on streamflow generation in a Mediterranean forested catchment, Journal of Hydrology, 660, 133469, https://doi.org/10.1016/j.jhydrol.2025.133469, 2025.

Kan, X., Cheng, J., and Hou, F.: Response of Preferential Soil Flow to Different Infiltration Rates and Vegetation Types in the Karst Region of Southwest China, Water, 12, 1778, 10.3390/w12061778, 2020.

Lee, E. and Kim, S.: Characterization of soil moisture response patterns and hillslope hydrological processes through a self-organizing map, Hydrol. Earth Syst. Sci., 25, 5733-5748, 10.5194/hess-25-5733-2021, 2021.

Li, B., Sprenger, M., Wyatt, B. M., Giménez, D., Hirmas, D. R., Ajami, H., Wiekenkamp, I., Groh, J., Nimmo, J. R., Amato, M. T., Singh, N. K., Crompton, O., Araki, R., Xu, T., and Sullivan, P. L.: Ubiquity and Causes of Soil Water Preferential Flow Across 17 Ecoregions, Geophysical Research Letters, 52, e2025GL118045, https://doi.org/10.1029/2025GL118045, 2025.

Li, X., Long, D., Slater, L. J., Moulds, S., Shahid, M., Han, P., and Zhao, F.: Soil Moisture to Runoff (SM2R): A Data-Driven Model for Runoff Estimation Across Poorly Gauged Asian Water Towers Based on Soil Moisture Dynamics, Water Resour. Res., 59, e2022WR033597, https://doi.org/10.1029/2022WR033597, 2023.

Lu, S., Liu, M., Yi, J., Zhang, H., and Wan, J.: Responses of soil moisture at different topographic positions to rainfall events along a steep subtropical forested hillslope, Hydrological Processes, 38, e15164, https://doi.org/10.1002/hyp.15164, 2024.

Marcotte, A. L., Limpens, J., Nunes, J. P., Howard, B., Hurley, A. G., Khamis, K., Krause, S., Croghan, D., Kourmouli, A., Leader, S., Singh, T., Stoof, C. R., Ullah, S., and Kettridge, N.: Enhanced Hydrologic Connectivity and Solute Dynamics Following Wildfire and Drought in a Contaminated Temperate Peatland Catchment, Water Resour. Res., 60, 10.1029/2023wr036412, 2024.

Nanda, A. and Safeeq, M.: Threshold controlling runoff generation mechanisms in Mediterranean headwater catchments, Journal of Hydrology, 620, 129532, https://doi.org/10.1016/j.jhydrol.2023.129532, 2023.

Nimmo, J. R., Wiekenkamp, I., Araki, R., Groh, J., Singh, N. K., Crompton, O., Wyatt, B. M., Ajami, H., Giménez, D., Hirmas, D. R., Sullivan, P. L., and Sprenger, M.: Identifying preferential flow from soil moisture time series: Review of methodologies, Vadose Zone Journal, 24, e70017, https://doi.org/10.1002/vzj2.70017, 2025.

Ortenzi, S., Massari, C., Ciabatta, L., Cencetti, C., Dionigi, M., Marchesini, I., Stelluti, M., and Di Matteo, L.: Leveraging SMAP-Based Soil Moisture to Identify Runoff Thresholds on Flash Flood–Prone Basins in the Mediterranean Region, J. Hydrometeorol., 26, 975-990, https://doi.org/10.1175/JHM-D-24-0143.1, 2025.

Pinos, J., Flury, M., Latron, J., and Llorens, P.: Routing stemflow water through the soil via preferential flow: a dual-labelling approach with artificial tracers, Hydrol. Earth Syst. Sci., 27, 2865-2881, https://doi.org/10.5194/hess-27-2865-2023, 2023.

Ran, Q. H., Wang, J., Chen, X. X., Liu, L., Li, J. Y., and Ye, S.: The relative importance of antecedent soil moisture and precipitation in flood generation in the middle and lower Yangtze River basin, Hydrology and Earth System Sciences, 26, 4919-4931, 10.5194/hess-26-4919-2022, 2022.

Salve, R., Rempe, D. M., and Dietrich, W. E.: Rain, rock moisture dynamics, and the rapid response of perched groundwater in weathered, fractured argillite underlying a steep hillslope, Water Resour. Res., 48, 10.1029/2012wr012583, 2012.

Singh, N. K., Emanuel, R. E., McGlynn, B. L., and Miniat, C. F.: Soil Moisture Responses to Rainfall: Implications for Runoff Generation, Water Resour. Res., 57, 10.1029/2020wr028827, 2021.

Uhlemann, S., Peruzzo, L., Chou, C., Williams, K. H., Wielandt, S., Wang, C., Falco, N., Wu, Y., Carr, B., Meldrum, P., Chambers, J., and Dafflon, B.: Variations in Bedrock and Vegetation Cover Modulate Subsurface Water Flow Dynamics of a Mountainous Hillslope, Water Resour. Res., 60, e2023WR036137, https://doi.org/10.1029/2023WR036137, 2024.

Wang, Y., Gao, L., Huang, S., and Peng, X.: Combined effects of rainfall types and antecedent soil moisture on runoff generation at a hillslope of red soil region, European Journal of Soil Science, 73, 10.1111/ejss.13274, 2022.

Zhang, G., Cui, P., Gualtieri, C., Bazai, N. A., Zhang, X., and Zhang, Z.: Increased nonstationarity of stormflow threshold behaviors in a forested watershed due to abrupt earthquake disturbance, Hydrol. Earth Syst. Sci., 27, 3005-3020, 10.5194/hess-27-3005-2023, 2023.

Zhang, J., Wang, S., Fu, Z., Wang, K., and Chen, H.: Characterizing rapid infiltration processes on complex hillslopes: Insights from soil moisture response to rainfall events, Journal of Hydrology, 644, 132110, https://doi.org/10.1016/j.jhydrol.2024.132110, 2024.

Zhang, J., Wang, S., Fu, Z., Wang, F., Wang, K., and Chen, H.: Regulation of Preferential Flow by Soil Thickness on Small Hillslopes With Complex Topography Through Intensive High-Frequency Soil Moisture Monitoring, Geophysical Research Letters, 52, e2024GL112674, https://doi.org/10.1029/2024GL112674, 2025.